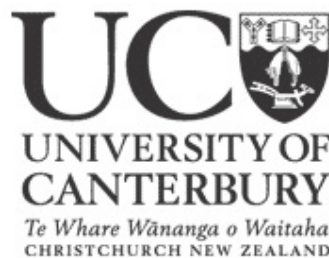Department of Physics and Astronomy, University of Canterbury,
Private Bag 4800, Christchurch, New Zealand

Controls of the Sea Ice Extent in the Ross Sea and Development of a Wireless Sensor Network

Robert Ward

UC
UNIVERSITY OF
CANTERBURY
Te Whare Wānanga o Waitaha
CHRISTCHURCH NEW ZEALAND

Master of Science Thesis

Supervisor: Dr. Adrian McDonald

Abstract

Polar sea ice is an important climatic variable. In the Arctic, the steady decrease in sea ice since the 1970's is a direct result of global warming. Due to the different land and ocean distribution in the Southern Hemisphere as well as circulatory effects from the ozone hole, Antarctica is isolated from these changes. These along with other factors have meant that Antarctic sea ice has experienced a slight increase over the same time period. Sea ice extent (SIE) is controlled by physical processes such as wind and ocean currents and temperature gradients, and these contribute to the seasonal and long term patterns in the formation and melting of sea ice. To date, climate models have had only limited success in modelling SIE and its geographic variation. The most commonly used measure to compare observations and models is the total sea ice area. However, observations suggest that the spatial variability of sea ice in response to climate drivers is complicated and differs markedly around the Antarctic. Various studies have suggested schemes for analysing SIE in terms of regional effects, although these schemes are generally somewhat arbitrary and may not be optimal for analysis of certain atmospheric circulation patterns.

This research examines a new method for Antarctic sea ice analysis. Using sets of satellite based observations of the SIE over the entire Antarctic continent, the edge of the sea ice can be described in terms of an ellipse. This provides an integrated measure of sea ice that also describes geographical variations while being mathematically simple to describe in terms of the five parameters that completely define an ellipse (centroid coordinates; major and minor axes lengths; rotation angle of major axis). This study demonstrates that the elliptical diagnostic analysis of sea ice captures seasonal and long term behaviour in sea ice well, and this behaviour was analysed in terms of atmospheric circulation patterns such as the El Niño Southern Oscillation (ENSO) and the Southern Annular Mode (SAM). Analysis of the ENSO and SAM on the Antarctic SIE show evidence that both are potentially important in controlling sea ice. Patterns in the ellipse parameters display results consistent with previous studies of the effect of ENSO and SAM on sea ice, but the significance of these forcings on sea ice remains an open question.

Part of this research involved development of a method to measure the atmospheric parameters that affect sea ice *in situ* in Antarctica, known as SNOW-WEB. The aim of the SNOW-WEB project is to design and implement a network of weather stations that can communicate wirelessly to each other, allowing near real-time measurement of weather variables over very high spatial and temporal resolutions, in the order of kilometres and minutes. Measuring the wind velocity, temperature and pressure over such high resolutions allow small scale atmospheric phenomena to be analysed in terms of their effects on sea ice.

The first deployment of the SNOW-WEB system was in January 2011 spanning the area between Scott Base and Windless Bight on Ross Island in Antarctica. One of the most important components of SNOW-WEB was its power supply system. A system was designed that would allow the SNOW-WEB nodes to operate continuously for over a week by a combination of lead acid batteries and a solar trickle charger. In addition, a research grade weather station was deployed as a reference and calibration point for the sensors on board each SNOW-WEB node. Due to the difficulties involved with Antarctic field work, the expectations for the performance of the SNOW-WEB were conservative, but the SNOW-WEB exceeded these comfortably.

Contents

List of Figures

List of Tables

Acknowledgements

I would like to thank the following people and organisations for helping me throughout my research:

Chapter 1

Introduction

This chapter details some of the previous studies of the Antarctic sea ice. In particular, the effects of atmospheric teleconnection patterns, such as the El Niño-Southern Oscillation (ENSO) and the Souther Annular Mode (SAM), on sea ice are described. Details of satellite measurement methodologies used for deriving sea ice concentrations and extents used in the majority of this thesis are described here as well as the details of particular sea ice datasets used in this study.

1.1   Sea Ice Overview

Sea ice is an important climate variable in both the Arctic and Antarctic, in particular due to the ice/albedo feedback mechanism which causes a polar amplification of climate change (Curry et al., 1995; Zwally et al., 1983; Walsh, 1983; Budyko, 1969). The albedo of bare sea ice is about 0.6, and this can increase to 0.9 with fresh snow cover. The albedo of open ocean is typically 0.1 or less, and as such there is greater heat uptake by the oceans than the snow/ice. This feedback mechanism is thought to be associated with decreases in snow and ice coverage causing an increase in surface temperature, hence further decreasing snow and ice cover and increasing surface temperature. Its extent is governed by many complex oceanic and atmospheric forcings, and monitoring and predicting its geographical and temporal extent is critical in climate studies.

It is important to distinguish between sea ice extent and sea ice area, as both are used in sea ice studies and are not equivalent terms. Sea ice extent is defined as the area of ocean with a sea ice concentration of at least 15% (Cavalieri and Parkinson, 2008b). This boundary criterion of 15% is not universal though, since various studies have used boundary criteria of between 10% and 30% (Parkinson et al., 1999; Zwally et al., 2002; Cavalieri et al., 2003). This usually does not affect sea ice extent measurements significantly since sea ice usually increases from 10% to more than 15% concentration less than 10km from the ice edge. Since most methods of measuring sea ice have less spatial resolution than 10km (typically 25×25km (Comiso, 1999, updated 2008; Long, 2004)), using different boundary criteria for the sea ice extent usually does not alter the measurement of sea ice extent significantly (Zwally et al., 1983). Sea ice area is defined as the sea ice extent excluding any polynya, and can be calculated by multiplying the sea ice extent by its concentration. However, reliable

data of sea ice concentration are historically not as extensive as data of sea ice extent since the earliest sea ice measurements were of sea ice extent rather than concentration (Zwally et al., 1983). Over long periods of data, sea ice extent and area display very similar trends, so analysis of sea ice extent alone is sufficient for our purposes.

In general, the physical processes that govern the annual growth and retreat of sea ice are well understood. Primarily, it is the seasonal cycle of solar insolation and temperature that drives this annual pattern. However, many other environmental factors affect sea ice extent and cover as well. How these various factors combine on long time scales and how regional variations in the factors affect the overall pattern is not well understood. In addition, how Antarctic sea ice interacts with global climate change is poorly understood (Zwally et al., 2002).

In the Arctic, there have been strong decreasing trends in both sea ice extent and areal coverage over the past 30 years, with statistically significant negative trends in almost every region of the Northern Hemisphere sea ice extent (Cavalieri and Parkinson, 2008b). These trends are also larger than predicted from general circulation models (Stroeve et al., 2007). However, this discrepancy is not unexpected since GCMs have traditionally modelled sea ice and its geographic variations with limited success (Walsh, 2009). Various studies have measured the decrease in Arctic sea ice as $-2.9 \pm 0.4\%$/decade between November 1978 and December 1996 (Cavalieri et al., 1997), $-2.7 \pm 0.5\%$/decade between 1979 and 1999 (Parkinson and Cavalieri, 2002), -4.6%/decade at the 99% confidence level from 1978-1995 (Bjorgo et al., 1997) and $-3.4 \pm 0.2\%$/decade from 1978 to 2006 (Comiso and Nishio, 2008). Cavalieri and Parkinson (2008b) measured the total negative trend as $-45,100 \pm 4,600$ km^2/a, or $-3.7 \pm 0.4\%$/decade in the yearly averages between 1978 and 2006, and negative trends are also present for each of the four seasons and twelve months.

In the Antarctic, sea ice trends are far less dynamic. In contrast to the large negative trends in the Arctic, several previous studies have shown no statistically significant long-term trends in Antarctic sea ice using passive microwave satellite observations since the interannual variability in sea ice cover is large compared to these trends (Gloerson and Campbell, 1991; Chapman and Walsh, 1993; Cavalieri et al., 1997). The sign of the trend in Antarctic sea ice coverage has been debated until recently. Increases have been measured as $1.3 \pm 0.2\%$/decade between 1978 and 1996 by Cavalieri et al. (1997), $0.98 \pm 0.37\%$/decade between 1979 and 1998 by Zwally et al. (2002), $0.9 \pm 0.3\%$/decade between 1978 and 2006 by Comiso and Nishio (2008) and 0.048×10^6km^2/decade by Liu et al. (2004). Decreases have been measured, but only by 1.1% at just 75% confidence (Bjorgo et al., 1997). Currently, the general consensus is that Antarctic sea ice coverage is slowly increasing, and this has been measured as $1.0 \pm 0.4\%$/decade for the total Antarctic sea ice extent between 1979 and 2006 (Cavalieri and Parkinson, 2008a).

The asymmetry between the Arctic and Antarctic sea ice is consistent with a modeled response to CO_2 induced global warming associated with increased heat uptake by the oceans at high southern latitudes (Cavalieri et al., 1997, 2003; Flato and Boer, 2001). The differing land and ocean distributions have been attributed to this asymmetry as well (Turner and Overland, 2009). The Arctic Ocean and hence sea ice is at a high latitude surrounded by land, and consequently experiences high levels of solar radiation during the summer, allowing the ice/albedo feedback mechanism to operate effectively. The Antarctic sea ice occurs at

lower latitudes and is surrounded by ocean. In addition, the Antarctic ozone hole has a profound effect on the circulations of the atmosphere and ocean at high latitudes, effectively isolating the continent from extrapolar circulation and increasing the westerly winds around the continent (Turner and Overland, 2009; Thompson and Solomon, 2002).

Multimodel general circulation models generally agree with sea ice behaviour in both the Arctic and Antarctic, although certain characteristics of the sea ice coverage are not reproduced well. In particular, the amplitude of the seasonal cycle of sea ice growth and decay is generally overestimated and a slight negative trend is displayed over decadal timescales, in disagreement with observations (Arzel et al., 2006).

Many studies have suggested that the spatial variability of Antarctic sea ice in response to various climate drivers is complicated and differs significantly from region to region around the Antarctic continent (Gloerson et al., 1993; Zwally et al., 2002; Stammerjohn et al., 2008). In particular, opposing regional trends seem to be a common feature of the response of Antarctic sea ice to various climatic forcings (Chapman and Walsh, 1993; Gloerson, 1995; Yuan and Martinson, 2000, 2001; Zwally et al., 2002). This suggests that using total sea ice extent and area metrics are unsuitable for representing the large regional variability in Antarctic sea ice. Zwally et al. (1983) suggested a set of regional sectors that can be used to examine spatial variability of sea ice (Figure 1.1), but this is not the only method of separating the Antarctic sea ice into regions. For example, others have used four 90°regions to examine the link between sea ice and the Southern Oscillation Index (Simmonds and Jacka (1995), see §1.2.1) and 5°increments to examine the Antarctic Circumpolar Wave (White and Peterson (1996), see §1.2.3). One limitation of the method by Zwally et al. (1983) is that since it uses five sectors, it is not optimal for examining patterns of wavenumber 2 or 3, both of which are seen in Antarctic sea ice analyses (White and Peterson, 1996; Lefebvre and Goosse, 2008).
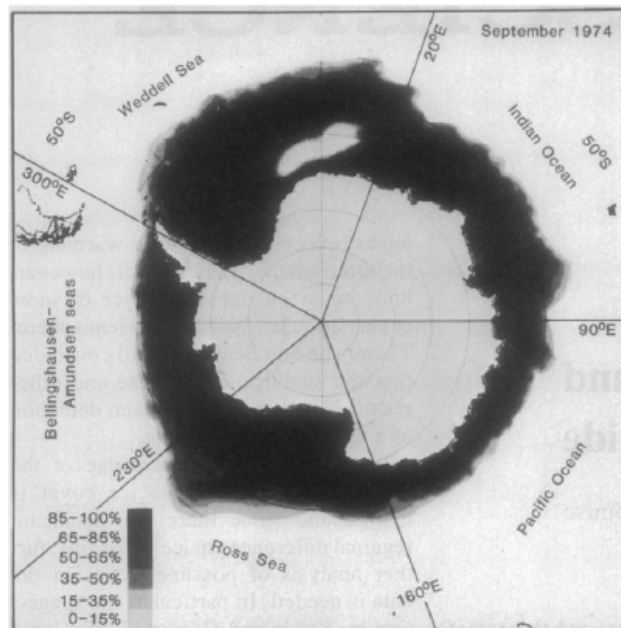
Figure 1.1: The regional sectors as defined by Zwally et al. (1983): Indian Ocean (20°E–90°E); Pacific Ocean (90°E–160°E); Ross Sea (160°E–230°E); Bellingshausen-Amundsen Seas (230°E–300°E); Weddell Sea (300°E–20°E) [after Zwally et al. (1983)]

1.2   Previous Studies of Teleconnection Patterns

The different behaviour in terms of sea ice extent and interannual variability between the Arctic and Antarctic suggests that each sea ice covered area is driven by different atmospheric and oceanic forcings. A large number of studies have been conducted on the various modes of atmospheric variability present in the Southern Hemisphere, but no clear consensus has been reached on the relative importance of each mode of variability (Yuan and Li, 2008).

1.2.1   El Niño-Southern Oscillation and the Antarctic Dipole

The El Niño-Southern Oscillation (ENSO) is a quasiperiodic climate pattern that manifests in the tropical Pacific Ocean about every five years. It is characterised by coupled variations in sea surface temperature in the eastern Pacific (El Niño (warm) and La Niña (cold)) and air pressure in the western Pacific (Southern Oscillation), but has global impacts such as variations in tropical precipitation and anomalies in the mean sea level pressure (MSLP) in the extratropics (Solomon et al., 2007). The Southern Oscillation is measured using the Southern Oscillation Index (SOI), which is a measure of the pattern between the pressures in the Indian Ocean/Australasian region and the southeastern tropical Pacific Ocean.

The Antarctic Dipole (ADP) is a quasi-stationary wave over the Drake Passage characterised by an out-of-phase relationship between ice and temperature anomalies, and it is associated with the ENSO in that it represents the greatest ENSO temperature anomaly outside of the tropical Pacific. During an El Niño event, the Pacific side of the dipole experiences warmer temperatures and less sea ice, while the Atlantic side experiences colder temperatures and more sea ice. The opposite is true for La Niña events (Yuan and Martinson, 2001).

The signature of the ENSO has been detected in polar ice fields in many studies (Simmonds and Jacka, 1995; White and Peterson, 1996; Harangozo, 2000; Yuan and Martinson, 2000, 2001; Kwok and Comiso, 2002; Rind et al., 2000; Martinson and Iannuzzi, 2003). Periodicities in the ice coverage at both hemispheric and regional scales have been observed to match those of the ENSO (Gloerson, 1995). However, the response to the ENSO is less significant in the Antarctic than the Arctic, and regional responses can vary greatly as well. In addition, Simmonds and Jacka (1995) suggests that the synchronous correlation between sea ice extent and the SOI is very small, which is not surprising given that physical mechanisms linking these two parameters would produce a delayed response.

Yuan and Martinson (2000, 2001) have shown that the ENSO can account for up to 34% of the variance in the sea ice extent anomalies ($\langle$SIE*$\rangle$), and that the $\langle$SIE*$\rangle$has even higher correlations with tropical Pacific precipitation and Indian Ocean sea surface temperature (SST). Correlations with global SST show four distinct patterns: An ENSO-like structure in the tropics; A teleconnection between the eastern Pacfic region of the Antarctic (Amundsen-Bellingshausen Sea) and the western-central tropical Pacific; The ADP across the Drake Passage; Meridional banding structures in the central Atlantic and Pacific emanating from the polar regions. It is the Pacific and Atlantic sectors of Antarctica (Amundsen-Bellinghausen and Weddell Seas) that show the greatest links between $\langle$SIE*$\rangle$and extrapolar climate, and this is shown most clearly in the ADP. Further work by Liu et al. (2002) has shown that

the covariance between the ADP and ENSO and hence sea ice variability can be linked to changes in the regional Ferrel cell due to altered meridional heat fluxes. The Ferrel cell is a major circulation feature of the atmosphere, along with the Hadley cell and the polar vortex. While the Hadley cell dominates circulation over the tropics and the polar vortices dominate circulation over the poles, the Ferrel cell controls circulation over the midlatitudes (Lorenz, 1967).

Kwok and Comiso (2002) examined the relationship between the SOI and Antarctic sea ice anomalies. They have concluded that strongest links between SOI and sea ice exist in the Amundsen, Bellingshausen and Weddell Seas. Here, positive SOI events are associated with lower sea level pressure, surface air temperature and surface sea temperature. Positive sea ice anomalies are located in the Ross and Amundsen Seas while negative sea ice anomalies are located in the Bellingshausen and Weddell seas.

In the 2003 austral summer, a record minimum extent of open water was observed in the Ross Sea. This has been attributed to the damming of the western Ross Sea by the iceberg C-19, but an anomalous atmospheric circulation typical of El Niño events contributed at least as much to this record low (Harangozo and Connolley, 2006).

1.2.2   Southern Annular Mode

The Southern Annular Mode (SAM) is the principal mode of variability in the Southern Hemisphere extratropics. It is essentially zonally symmetric (hence "annular") with a wavenumber three pattern superimposed and is associated with synchronous pressure anomalies of opposite sign in the mid- and high-latitudes (Solomon et al., 2007). It accounts for about 10% of the total variance in the monthly mean global atmospheric mass.

Hall and Visbeck (2002) studied how the atmosphere, ocean and sea ice respond to the SAM by performing a 15,000 year integration of a coarse resolution coupled ocean-atmosphere model, and have concluded that SAM is an important source of large-scale variability in the Southern Hemisphere ocean. They show that ocean and sea ice variations are tightly in phase with the SAM on interannual to centennial timescales and that these fluctuations constitute a significant fraction of the ocean variability throughout the entire Southern Hemisphere polewards of 30°S. During phases of positive SAM, the circumpolar current around Antarctica becomes more intense, advecting sea ice northwards and hence increasing sea ice coverage. The opposite occurs during negative SAM events. This has also been observed by Liu et al. (2004), and they also note that these changes are qualitatively opposite what is experienced during positive ENSO events. However, in contrast to Hall and Visbeck (2002), Liu et al. (2004) argue that ENSO and SAM cannot totally explain regional ice trends. Furthermore, study by Yuan and Li (2008) shows that the ENSO and SAM are the dominant factors leading to a strong interaction between the atmosphere and the Antarctic sea ice extent, supporting the conclusions drawn in Hall and Visbeck (2002).

Lefebvre et al. (2004) have studied the response of Antarctic sea ice to the SAM and concluded that this response consists of an annular and non-annular mode. The non-annular mode seems most important in terms of sea ice cover and the annular component strongly affects the patterns of upper ocean circulation. When the SAM is in a positive phase, the annular component is associated with a northwards Ekman drift, which is the motion of

water driven by wind currents. This drift is also linked to downwelling at about 45°S and an upwelling around the Antarctic continent. The non-annular component has a significant impact on the regional scale, and the pressure patterns associated with the SAM cause an increase in sea ice in the Ross and Amundsen Seas and a decrease in sea ice in the Weddell Sea and around the Antarctic Peninsula.

The response of the coupled ocean-atmosphere-ice system to the SAM has been examined by Sen Gupta and England (2006). They show that drag forces associated with SAM surface wind and ocean circulation anomalies, as well as various other thermodynamic forcings, affect the advection, formation and melting of sea ice. The SAM-induced change in sea ice coverage is well explained at most locations by anomalous ice advection, and the sea ice velocity generally has an eastward component in agreement with SAM-related stresses from the ocean and wind. In addition, a maximum in the response of sea ice to SAM is seen at between 1- and 5-month lags, depending on location. These anomalies are also very persistent. The maximum response tends to occur after the time of maximum external atmospheric and oceanic forcing, and this suggests that an ice/albedo feedback mechanism operates to enable this persistence due to the inertia in the system.

Stammerjohn et al. (2008) have shown that regional sea ice trends result largely from wind-driven sea ice changes. These have been associated with increasing positive SAM phases with coincident La Niña events. This leads to a strengthening in northerly winds in the Antarctic Peninsula and Bellingshausen Sea, causing an earlier wind-driven sea ice retreat and a later sea ice advance. In contrast, the strengthening zonal circulation and persistent northwards Ekman sea ice drift associated with positive SAM has caused later sea ice retreat and earlier sea ice advance in the Ross Sea. This is consistent with other studies showing that sea ice extent has generally increased in the Ross Sea and decreased on the Antarctic Peninsula (Turner et al., 2009).

1.2.3   Antarctic Circumpolar Wave

The Antarctic Circumpolar Wave (ACW) is a self-sustaining eastward propagating wave first identified by White and Peterson (1996). It links sea level atmospheric pressure, sea ice extent, wind stress and sea surface temperature in a wave with a period of 4–5 years that encircles the pole about every 8–10 years, hence showing a wavenumber 2 pattern. The interannual variability of the four parameters seem to be coupled and observations show that these coupled anomalies of the parameters propagate eastward. The ACW has been the source of much debate concerning its generation mechanisms (White et al., 1998; Qiu and Jin, 1997), persistence (Bonekamp et al., 1999) and even existence (Christoph et al., 1998; Park, 2001).

However, work by Park et al. (2004) suggests little evidence for the ACW. They compared the links between the sea ice extent and both the ACW and ENSO, which can be thought of as propagating and stationary components, respectively, of several atmospheric and oceanic variables. They found that the ACW contributed as little as 25% of the sea ice variability as compared to the ENSO contribution of 65%. They also identified that the propagating component rapidly dissipates and cannot complete the circumpolar journey. It is also intermittent in phase, so the ACW has largely fallen out of favour as an explanation

for Antarctic sea ice variability.

1.2.4   Other Atmospheric Forcings

Yuan and Li (2008) have studied the four major climate modes that influence Antarctic sea ice. They are the Pacific South American pattern (PSA), the SAM, the Semi-Annual Oscillation (SAO) and the quasi-stationary wave-3 pattern (Zonal Wave-3, or ZW3). Out of these, the PSA has the greatest impact on sea ice. The PSA is the climate pattern that most directly relates to the ENSO and is manifested in the Antarctic Dipole (ADP) region of the Western Hemisphere, specifically around the Drake Passage at the southern tip of South America. The ZW3 pattern has a similar influence on the sea ice in the ADP regions suggesting that there are positive interactions between the ZW3 and PSA patterns. The SAM and SAO are not as strongly related to sea ice variability here, but it must be noted that this particular study does not examine regional responses to climate modes, only global responses. They also found that sea ice usually responds to large-scale atmospheric anomalies with a delay of about two months.

Lefebvre and Goosse (2008) studied the response of Antarctic sea ice to the variability of the atmosphere between 1979 and 2004 using both model and observational data. They concluded that the classical modes of southern hemisphere atmospheric variability (SAM, ENSO, ZW3, SAO) do not explain a large part of the winter sea ice extent variability integrated over the entire Southern Ocean. However, a regression between the sea ice and atmospheric pressure shows a pattern of low pressure areas over the south Atlantic, Indian and southwest Pacific Oceans which does not correlate significantly to any known mode of atmospheric variability. In addition, there is no clear link between the centres of action of this pattern, nor is the correlation between different sectors of sea ice extent high. This suggests that the Antarctic sea ice does not behave as a single entity, but rather each region of sea ice contributes to the overall variability of sea ice extent independently.

The ZW3 has been studied further by Raphael (2007). That work concludes that ZW3 forces an alternating pattern of equatorward (colder) and poleward (warmer) air flow. In regions where there is a cold air flow, the sensible heat flux is positive and this causes a heat loss in the ocean and a corresponding growth and expansion of sea ice. The reverse is true in regions with warm air flow. The effect of ZW3 is most noticeable in the austral fall and early winter in the Ross and Weddell Seas.

1.3   Measuring Sea Ice

While in situ measurements were used before the space age, satellite observations are currently the main form of measuring sea ice. In particular, Antarctic sea ice is very poorly measured before 1973 when the Electrically Scannning Microwave Radiometer (ESMR) mounted on the Nimbus V satellite was first used to observe sea ice (Wilheit, 1972). In fact, only two data sources exist from prior to 1973: the monthly sea ice extent climatology for 1929–1939 published by the Deutsches Hydrographisches Institute (1950) and that of Tolstikov (1966) that summarises observations from Russian expeditions between 1947 and 1962 (Rayner

et al., 2003). These two sources are poor quality as they are compiled from observations from ocean expeditions and as such do not include sea ice concentration information, nor do they have records for the entire sea ice around Antarctica.

1.3.1   Passive Microwave Radiometry

Since 1978, many satellites have observed sea ice in both the Arctic and Antarctic using passive microwave radiometry. The Bootstrap Sea Ice Concentrations from Nimbus-7 SMMR and DMSP SSM/I dataset (Comiso, 1999, updated 2008) is used as a primary data source for this study. This dataset uses a compilation of sea ice concentration data from instruments on four of these satellites: The Scanning Multichannel Microwave Radiometer (SMMR) mounted on the Nimbus-7 meteorological observatory which operated from 26 October 1978 to 20 August 1987 (Madrid, 1978); and the Special Sensor Microwave Imager (SSM/I) mounted on three Defense Meteorological Satellite Program (DSMP) satellites, namely -F8, -F11 and -F13 (Dubach and Ng, 1988). -F8 operated from 9 July 1987 to 18 December 1991, -F11 operated from 3 December 1991 to 31 December 1996 and -F13 operated from 5 May 1995 to the present day. SSM/I instruments were mounted on the DSMP -F10, -F12 and -F15 satellites as well, although these are not included in the Bootstrap data. The next generation of the SSM/I, the Special Sensor Microwave Imager/Sounder (SSMI/S) is mounted on the DSMP -F17 satellite and these data are currently being integrated into the Bootstrap dataset.

The SMMR and SSM/I instruments passively sense microwave emissions at an incidence angle of about 53°and an altitude of about 800km. At microwave frequencies, the radiance varies linearly with temperature, in accordance with the Rayleigh-Jeans law, and this radiance is usually measured in brightness temperature. The sea ice concentration C_I can then be calculated using the following linear equation (Zwally et al., 1983):

$$T_B = T_I C_I + T_O(1 - C_I) \tag{1.1}$$

T_B is the brightness temperature measured by the instrument, T_I and T_O are the brightness temperatures of the ice and ocean, respectively. The constant of proportionality in the linear relationship is the emissivity, which provides information about the physical properties of the emitting surface. The emissivity and hence brightness temperature is dependent on surface, subsurface and atmospheric conditions, and this is reflected in the frequency and polarisation of the microwave radiation. Equation 1.1 suggests that measurements at one frequency are sufficient for sea ice measurement if the emissivities of the ocean and ice are unique and the surface temperature is known. In practice, this cannot be assumed since pack ice is inhomogeneous in regard to temperature and emissivity (Comiso, 1983; Parkinson et al., 1987). This inhomogeneity is due to the differing physical properties of the sea ice and causes changes in the brightness temperature depending on the frequency and polarisation measured. Therefore, the multichannel capability of the instruments is required to discriminate between different surfaces and atmospheric effects and to allow further geophysical information to be obtained about the surface.

1.3.2 Radar Scatterometry

Another method of measuring sea ice is that of radar scatterometry, measuring reflected microwave radiation rather than emitted microwave radiation (Long, 2004). The SeaWinds scatterometer is an instrument mounted on NASA's Quick Scatterometer (QuikSCAT) satellite that uses this technique to measure sea ice extent, and these data are used in the NASA Satellite Climate Record Pathfinder Arctic and Antarctic Ice Extent from QuikSCAT dataset. The SeaWinds instrument transmits pulses of microwave energy in the Ku-band, specifically 13.4 GHz, towards the earth and measures the magnitude of the return echo, which depends on the electrical properties and surface roughness of the material measured. While the SeaWinds instrument was originally designed to measure near-surface winds over the ocean, it proved useful for ice and land measurements as well, since Ku-band radar backscatter is extremely sensitive to the differences between ice and open water so sea ice extent is easy to measure (Kramer, 1994; Remund and Long, 1998; Remund, 1999; Remund and Long, 2000; Long et al., 1993). The QuikSCAT satellite was lost on 23 November 2009 when the bearings allowing its radar antenna to rotate failed.

1.4 Sea Ice Extent and Concentration Datasets

Three primary datasets are used in this study to ensure that the ellipse fitting algorithm produces consistent results. Since each source measures sea ice in a different way, and presents the measurements in different formats, obtaining similar results when applying the algorithm to each dataset should be a good indicator that the algorithm works as intended.

1.4.1 Hadley Centre Sea Ice and Sea Surface Temperature dataset

The Hadley Centre Sea Ice and Sea Surface dataset (Hadley) is a compilation of sea ice concentration and sea surface temperature data from many sources that span from 1870 to 2009 (Rayner et al., 2003). It has a spatial resolution of $1° \times 1°$ and a temporal resolution of one month. The data from 1978 onwards is compiled from various satellites including those used in the Bootstrap dataset (§1.4.2), but before the 1970's only in situ measurements were used, for example Deutsches Hydrographisches Institute (1950) and Tolstikov (1966) provide limited Antarctic sea ice measurements for before 1978. The data before 1978 are considered to be only a general indication of sea ice and as such are not considered in this study.
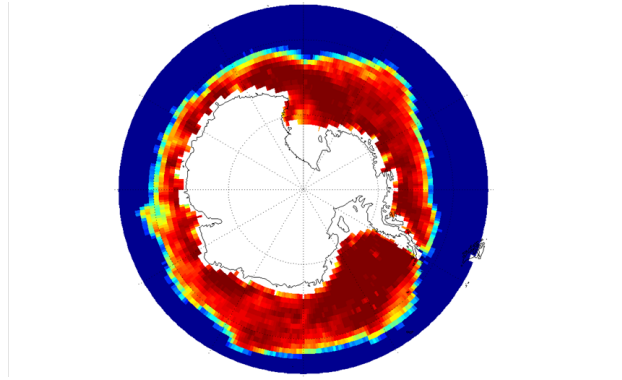
Figure 1.2: Example measurement of sea ice from the Hadley data for October 1990. Sea ice concentration is reported with a spatial resolution of 1°×1°and a temporal resolution of one month.

1.4.2 Bootstrap Sea Ice Concentrations from Nimbus-7 SMMR and DMSP SSM/I

The Bootstrap Sea Ice Concentrations from Nimbus-7 SMMR and DMSP SSM/I (Bootstrap) is a dataset of sea ice concentrations derived from passive microwave radiometry instruments aboard four meteorological satellites (Comiso (1999, updated 2008), also discussed in Comiso and Nishio (2008)): The Scanning Multichannel Microwave Radiometer (SMMR) on board the Nimbus-7 Satellite (Madrid, 1978) and the Special Scanning Microwave Imager (SMM/I) on board the Defense Meteorological Satellite Program (DMSP) satellites -F8, -F11 and -F13 (Dubach and Ng, 1988). It is available in daily measurements and monthly mean measurements, and daily measurements are used here. While the spatial resolution is about 25×25km, this changes slightly depending on the distance of the measurement from the South Pole, so each pixel has an area of between 460 and 665 km^2.
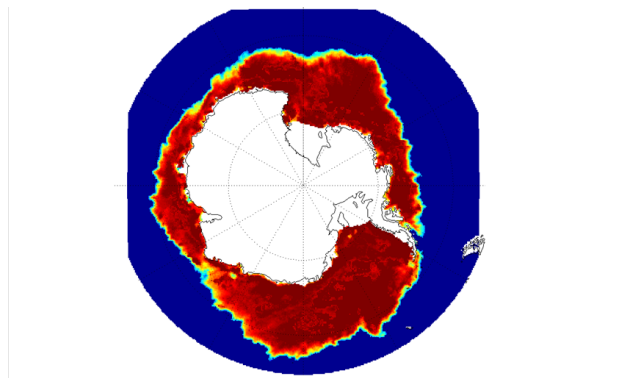
Figure 1.3: Example measurement of sea ice from the Bootstrap data for 19th July 2003. Sea ice concentration is reported with a spatial resolution of approximately 25×25km depending on the latitude. The data have a temporal resolution of one day.

1.4.3 NASA SCP Arctic and Antarctic Ice Extent from QuikSCAT

The NASA SCP Arctic and Antarctic Ice Extent from QuikSCAT (QuikSCAT) is a dataset of sea ice extent derived from the SeaWinds scatterometer on board the NASA Quick Scatterometer satellite. This dataset is slightly different to the Bootstrap and Hadley datasets in that it does not provide sea ice concentration data, only sea ice extent. Since this satellite was a "quick recovery" mission to replace the NASA Scatterometer flown on Japan's Midori satellite which unexpectedly failed in 1997 (Graf et al., 1998), it did not run for a very long time compared to other datasets. This particular dataset only runs for five years from 1999 to 2004, and as such is only used as a source to verify the performance of the ellipse fitting algorithm.
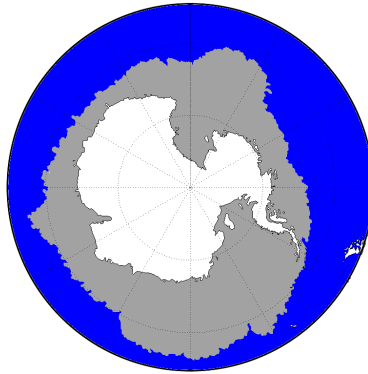
Figure 1.4: Example measurement of sea ice from the QuikSCAT data for 23rd August 2001. Rather than sea ice concentration data, QuikSCAT data is of sea ice extent only, so sea ice areas cannot be calculated here. The data have a spatial resolution of approximately 20×30km and a temporal resolution of one day.

1.4.4 Summary of Datasets

Table 1.1: Summary of the temporal and spatial resolutions of the three datasets used. The Hadley data are of significantly lower spatial and temporal resolution than the Bootstrap and QuikSCAT data, but this does not affect the elliptical diagnostic analysis. The QuikSCAT data run for only five years and as such are not used extensively in this research.

Dataset	Spatial Resolution	Temporal Resolution	Start Date	End Date
Hadley	$1° \times 1°$	Monthly	1 January 1871	31 December 2008
Bootstrap	About 25×25km	Daily	26 October 1978	31 December 2007
QuikSCAT	About 20×30km	Daily	19 July 1999	31 December 2004

Chapter 2

Elliptical Diagnostics of Antarctic Sea Ice

This chapter describes the methodology for fitting ellipses to the Antarctic sea ice extent, with the particular mathematical details described in Appendix A. The performance of the ellipse fitting algorithm is assessed by comparing the ellipses produced by each dataset with each other as well as with observational data.

2.1   Motivation for Elliptical Diagnostics

Many studies have shown that the behaviour and response of Antarctic sea ice to various atmospheric and oceanic forcings can vary greatly by region (Gloerson et al. (1993); Zwally et al. (2002); Stammerjohn et al. (2008), also see §1.1). Studies of Antarctic sea ice as one entity potentially do not capture the regional behaviour of sea ice. In addition, small-scale phenomena such as ice tongues and polynya (areas of open sea within sea ice cover) have been shown to affect how the sea ice behaves as a whole (Reddy et al., 2007; Rintoul et al., 2008). To overcome this limitation of sea ice analysis, several methods of breaking up the Antarctic sea ice into smaller regions have been used.

The scheme devised by Zwally et al. (1983) divides the Antarctic sea ice into five regions according to various geographic features such as the Antarctic Peninsula (see Figure 1.1). However, the regions in this method are somewhat arbitrary, and since there are five regions, changes in these regions linked to the wavenumber 2 and 3 patterns identified in previous Antarctic sea ice analyses may be difficult to observe (White and Peterson, 1996; Lefebvre and Goosse, 2008). Other authors such as Simmonds and Jacka (1995) and White and Peterson (1996) divided the sea ice into four 90° sectors and 72 5° sectors, respectively. Since the regional response of Antarctic sea ice to various atmospheric and oceanic forcings is complicated, a method of measuring sea ice variability which identifies geographic variations is potentially useful for sea ice analysis. The schemes devised in Zwally et al. (1983), Simmonds and Jacka (1995) and White and Peterson (1996) allow regional analysis of sea ice behaviour, however these schemes are somewhat arbitrary in nature and may not be entirely behaviour of sea ice. An integrated measure of total sea ice variability which also accounts for geographic variability is therefore advantageous.

Elliptical diagnostics provide a potential integrated measure of how sea ice behaves without relying on dividing sea ice into arbitrary sectors that may not accurately capture sea ice behaviour over the entire continent. Since the Antarctic sea ice is roughly elliptical for a large portion of the year, fitting an ellipse instead of some other shape is a logical choice. This work is inspired by Waugh (1997), who applied a similar ellipse fitting technique to the polar vortices. He found that the temporal and spatial characteristics of the vortices can be usefully quantified in terms of how the ellipse parameters change. Since Antarctic sea ice shows similar spatial and temporal variations both interannually and over longer time periods, the ellipse parameters here should show similar behaviour. This allows, for example, geographic variations in sea ice cover to be analysed instead of a simple total area measure.

An ellipse is a simple shape to parameterise. It can be completely defined with five parameters:

- Coordinates of the ellipse centroid in either Cartesian or polar format.

- Lengths of the major and minor axes.

- Rotation angle of the ellipse.

By fitting an ellipse to the ice edge, defined here as the set of northernmost points where sea ice concentration reaches $\geq 15\%$, the sea ice can be described in terms of these parameters. The threshold sea ice concentration of $\geq 15\%$ is chosen as it is a standard threshold used in previous sea ice studies (Zwally et al., 1983).

2.2   The Ellipse-Fitting Algorithm

The first step in the algorithm was to determine the ice edge from sea ice concentration data. For the Hadley and Bootstrap data, this was done by dividing the sea ice into one degree wide slices and finding the northernmost point in each slice with a reported sea ice concentration of $\geq 15\%$. The QuikSCAT data is provided as latitude and longitude coordinates of the sea ice edge, so no ice edge detection was necessary here. The threshold of $\geq 15\%$ is used here since it is a standard threshold value for sea ice. Remund and Long (1998) note that a threshold value of 30% provides the best match between areas derived from the QuikSCAT and SSM/I instruments, although some seasonal variation is seen due to the differences in sensitivity between passive and active sensors to sea ice. The analysis here does not show any significant differences in areas derived from ellipses using thresholds of 15% or 30%. As examined by Parkinson et al. (1999), the exact sea ice concentration threshold used does not affect measurements significantly due to the large gradient in sea ice concentration observed at the boundary of the sea ice extent.

After detection, the sea ice edge data were projected onto a plane using the polar stereographic projection:

$$x = \frac{\cos(\lambda)\cos(\phi)}{1 - \sin(\lambda)} \tag{2.1}$$

$$y = \frac{-\cos(\lambda)\sin(\phi)}{1 - \sin(\lambda)} \tag{2.2}$$

where λ is the latitude and ϕ is the longitude. The non-iterative ellipse fitting algorithm described in Taubin (1991) and summarised in Appendix A is then applied to the projected ice edge data. While not the most accurate method of fitting an ellipse (Kanatani and Rangarajan, 2011) it is still one of the most accurate non-iterative algorithms. Since it is non-iterative, it is computationally very efficient and does not suffer from any issues related to convergence from poor selection of initialisation values inherent in iterative ellipse fitting methodologies.

The ellipse was then reprojected back onto a sphere using the reverse polar stereographic projection:

$$\phi = \sin^{-1}\left[\frac{-2}{x^2 + y^2 + 1} + 1\right] \tag{2.3}$$

$$\lambda = -\tan^{-1}\left(\frac{y}{x}\right) \tag{2.4}$$

Many other ellipse-fitting routines were examined and the results were essentially the same for all the algorithms, therefore the results presented here are not sensitive to the algorithm used. It should be noted that the ellipse fitting methodology detailed in Waugh (1997) in his study of the polar vortices is similar to the technique used here.

Since the fitted ellipse is returned as a set of algebraic coefficients (Equation A.1), the five variables that completely define an ellipse must be derived using Equations A.11. . . A.15. These can then be analysed to examine seasonal variations and long-term trends in the sea ice cover. The area of the ellipse is easily calculated, but must be corrected by ignoring the area of Antarctica and the permanent ice shelves (approximately $15 \times 10^6 \mathrm{km}^2$) so that it is the area of only the sea ice.

An example of the ellipse fitting for a specific date for each dataset is shown in Figure 2.1 and an example of how the ellipse changes over a year with the sea ice is shown in Figure 2.2. Figure 2.1 shows that the ellipse fitting algorithm produces very similar results for each of the three datasets. It must be noted that the ellipse for the Hadley data (Figure 2.1a) is fitted for all of August due to it's monthly temporal resolution, not just the 23rd, so it is slightly different.

Figure 2.2 shows that fitting an ellipse to the ice edge is a reasonable assumption, although the fit for March (Figure 2.2a) is not as good as for other months. This is due to the fact that sea ice is at a minimum around February and March and as such the shape of the sea ice is dominated by the Antarctic coastline rather than being more elliptical as it is over the rest of the year. This means that the edge of the sea ice in general no longer forms an ellipse and as such the ellipse fitting algorithm is not expected to perform well. The correlation coefficients between the ellipse edge and the sea ice concentration edge for the four dates displayed in Figure 2.2 are: 0.74 (a), 0.87 (b), 0.89 (c) and 0.92 (d). These high values for the correlation coefficients further demonstrate that ellipses provide a relatively good approximation to the geographic form of the Antarctic sea ice.
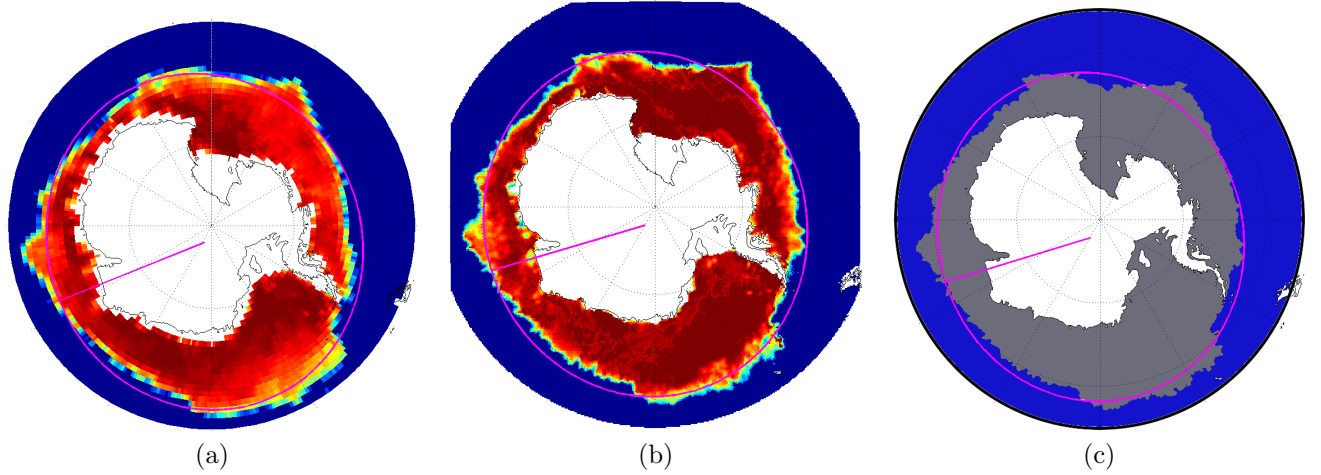
Figure 2.1: Example ellipse fits (pink) for 23rd August 2001 for the three datasets: Hadley (a), Bootstrap (b), QuikSCAT (c). The semi-minor axis is marked and this shows both the rotation angle and the location of the centroid of each ellipse. It must be noted that the Hadley ellipse (a) is for the month of August 2001 rather than just the 23rd of August since the Hadley data is only available monthly rather than daily like the other two datasets.

2.3 Assessing Algorithm Performance

One way of assessing the performance of the ellipse fitting algorithm is to compare the results with known sea ice behaviour. If they match well, then that suggests that elliptical diagnostics are a valid method of analysing sea ice. Since the only directly comparable parameter between the ellipse diagnostics and the data itself is the area, this is chosen as the particular metric by which the validity of the algorithm is determined. To calculate the sea ice area directly for comparison purposes, all the pixels in each sea ice image with sea ice concentrations greater than 15% were multiplied by their respective areas and summed.

An example of this comparison is shown for the QuikSCAT data for the year 2000 (Figure 2.3), and the patterns shown are typical for every year for all three datasets. The two areas shown in Figure 2.3 display excellent correspondence, and this suggests that elliptical diagnostics have some merit. A minimum occurs in the ellipse area around February/March and a maximum occurs around September/October, and this is supported by other sea ice observations (Cavalieri and Parkinson, 2008a). In addition, Gloerson et al. (1993) amongst others have indicated that the February minimum is followed by a gradual expansion until the September/October maximum, which in turn is followed by a rapid decay through November and December. As this pattern is observed in the ellipse area, this further suggests the ellipse diagnostics are valuable.

Figure 2.4 shows the comparisons between the areas derived from ellipses and data for each entire dataset and the correlation and linear fit coefficients of each comparison are shown in Table 2.1. Both the correlations and gradients are very close to unity, suggesting that the ellipse fitting performs very well for all datasets at all times of year. This is somewhat surprising for periods where sea ice extent is at a minimum since the sea ice at periods of minimum extent is typically dominated by the Antarctic coastline rather than being more elliptical as it is at other times of year (see Figure 2.2a). However, since only the areas are

16
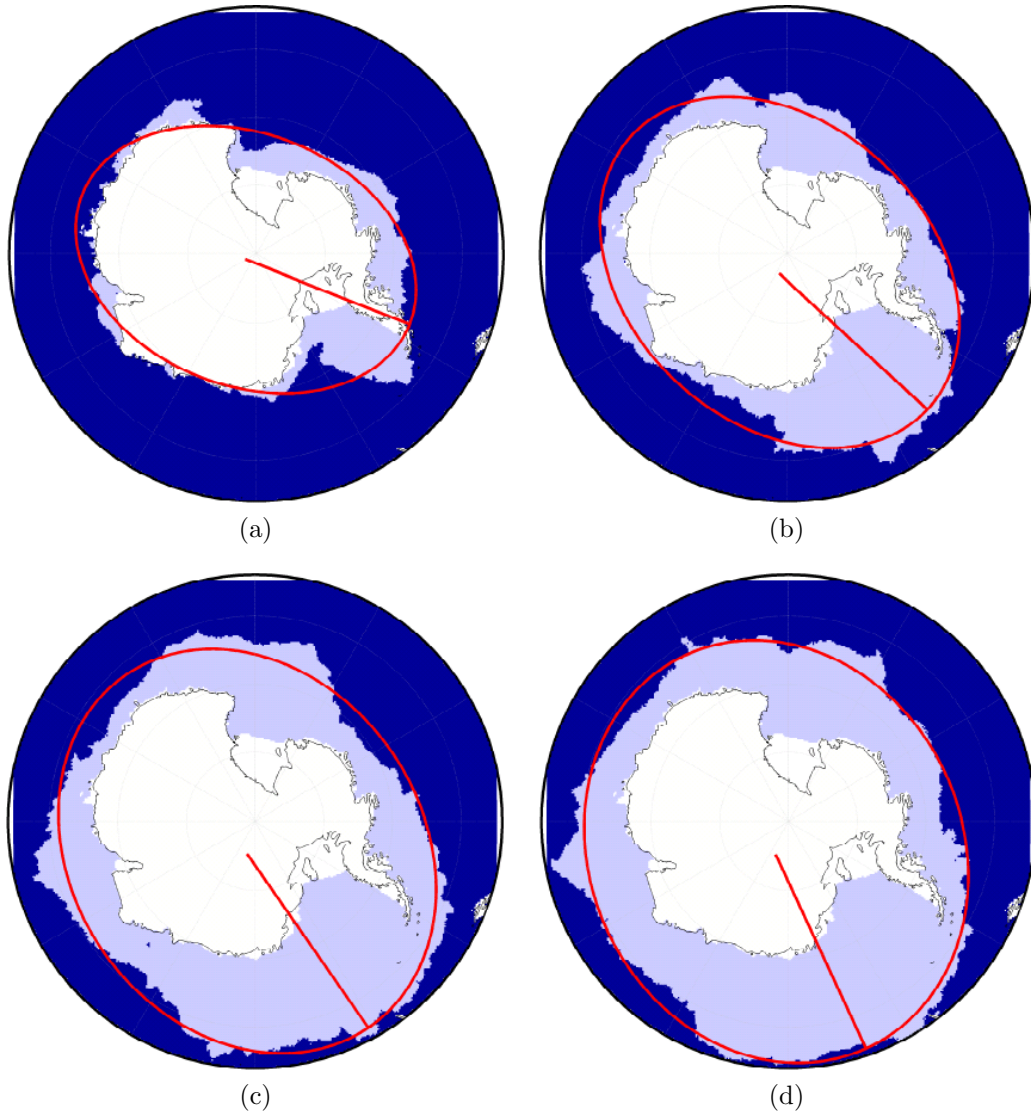
Figure 2.2: Example ellipse fits over a year from the Bootstrap data, for 30th March 1980 (a), 1st June 1980, (b), 31st July 1980 (c), 1st October 1980 (d), respectively.

Table 2.1: Linear fit and correlation coefficients for each dataset plus the coefficients for the Bootstrap/QuikSCAT intercomparison

Dataset	Gradient	Intercept (10^6km^2)	Correlation Coefficient
Hadley (2.4b)	1.1	-0.4	0.99
Bootstrap (2.4a)	0.98	-0.3	0.97
QuikSCAT (2.4c)	0.98	0.4	0.95
Bootstrap/ QuikSCAT (2.4d)	0.85	1.6	0.91

being compared here instead of the actual shape of the sea ice, this may not be an accurate comparison between the ellipse and the sea ice for this particular time of year.

For reference purposes, the areas derived from the data for Bootstrap and QuikSCAT were compared in the same way. As seen in Figure 2.4d, the comparison is not as good as any of the ellipse/data comparisons for the individual datasets. The discrepancies between the Bootstrap and QuikSCAT datasets have been noted previously, and are attributed to differences in sensitivity to sea ice between active and passive sensors used on the different satellites flown for each mission (Remund and Long, 1998). Even though the Bootstrap/QuikSCAT intercomparison displays the lowest correlation here, it is still very high, and agrees with the high correlations between sea ice extent measurements from different sensors identified in Allen and Long (2006).

Linear fits were applied to these comparisons to determine if there was any significant bias in the ellipse fitting algorithm. While none of the linear fits have an intercept at the origin, the intercepts are all very small, suggesting there is little bias in the ellipse areas. The Bootstrap, Hadley and QuikSCAT data have intercepts of -0.3×10^6km^2, -0.4×10^6km^2 and 0.4×10^6km^2 respectively, suggesting that the ellipse fits are very slightly under- and overestimating the sea ice extent, respectively. Figure 2.3 seems to support this as the QuikSCAT ellipse areas seem to be consistently greater than the data areas. However, the differences in areas between the ellipses and the direct calculation are so small that this would have little if any effect on the further analysis of the elliptical diagnostics. It is also encouraging to note that the Hadley ellipses have a similar bias to the other two datasets even though it's spatial and temporal resolutions are far less than those for the other datasets, suggesting that the quality of the ellipse fitting is relatively insensitive to changes in data resolution.

Since the ellipse fitting algorithm appears to perform well in terms of capturing established sea ice behaviour, the additional information it provides in terms of geographical sea ice extent should prove useful.
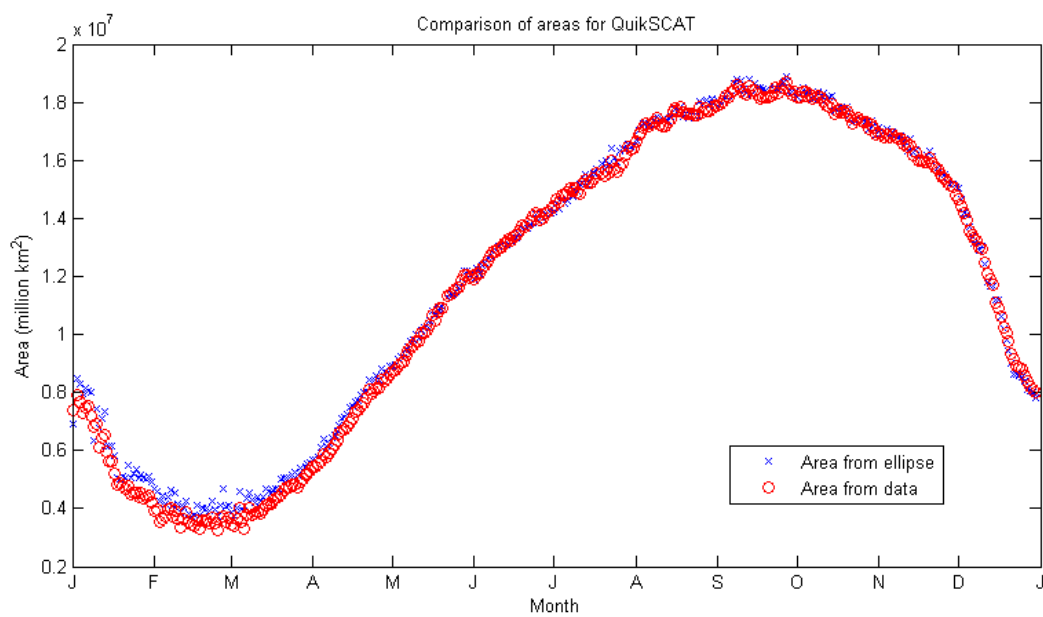
Figure 2.3: Comparison of the areas of sea ice derived daily from a direct (red circles) and ellipse (blue crosses) calculation for the QuikSCAT data from 2000.
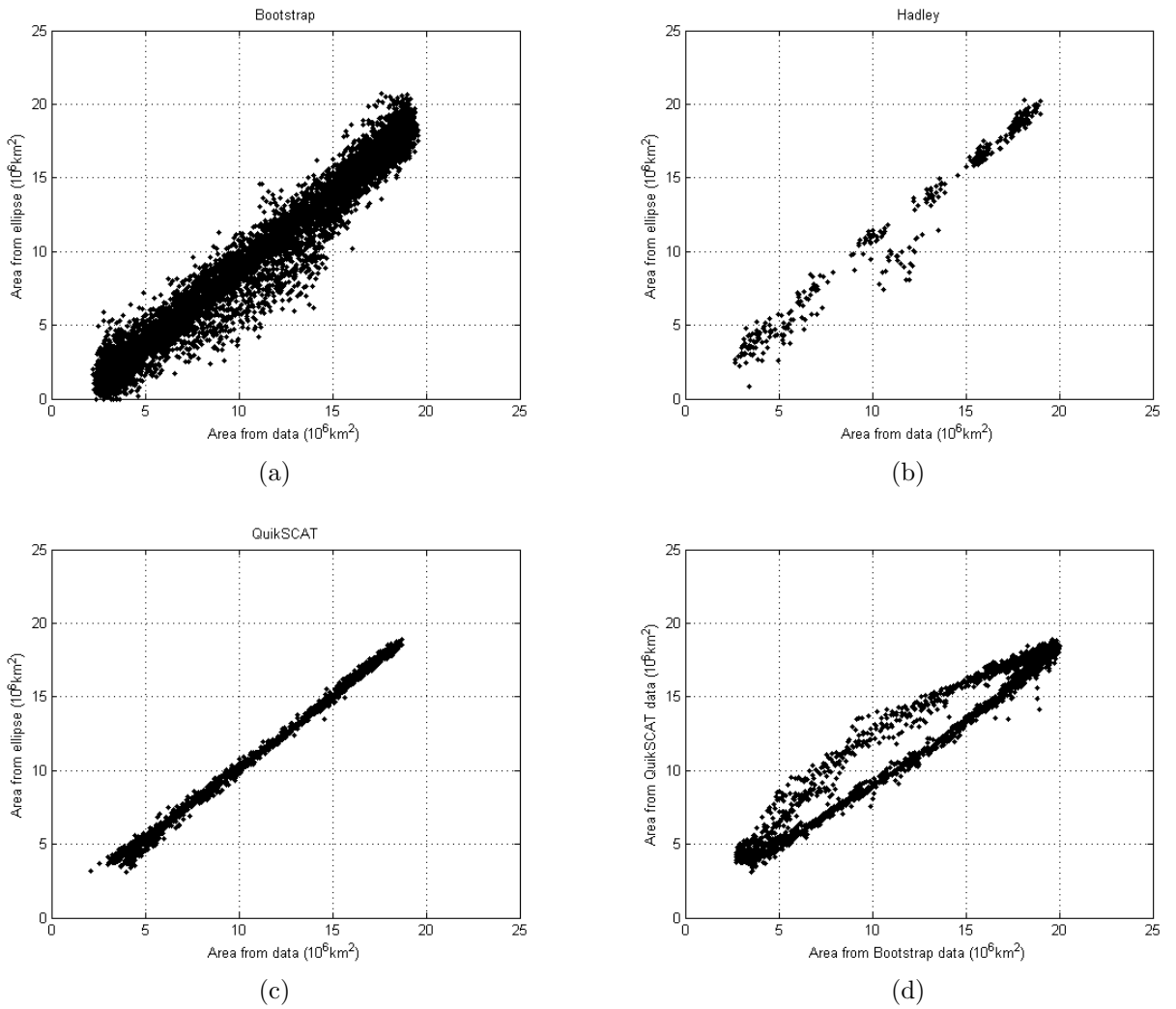
Figure 2.4: Comparisons between the areas derived directly and from the ellipse fitting methodology for each entire dataset: Bootstrap (a); Hadley (b); QuikSCAT (c). (d) shows the comparison of the areas derived from the QuikSCAT and Bootstrap datasets.

Chapter 3

Analysis of Ellipse Parameters

This chapter analyses the seasonal and long term patterns and trends in the ellipse parameters. Initial comparisons are made with the ENSO and SAM and these comparisons are used to make initial conclusions about the relative importance of the effects of each teleconnection pattern on the Antarctic sea ice extent.

3.1 Seasonal cycles in ellipse parameters

Figure 3.1a shows the mean annual cycle in the ellipse parameters, displaying excellent correspondence between the parameters extracted from the three datasets. The most obvious feature of each is that they all display very strong annual periodicities corresponding to the yearly cycle of sea ice growth and retreat. This seasonal cycle due to the various solar, atmospheric and oceanic forcings is well documented (Cavalieri and Parkinson, 2008b) and dominates the variations seen in sea ice and the ellipse parameters. The strong seasonal patterns in the ellipse parameters suggest that the elliptical diagnostic model captures the sea ice behaviour well. The major and minor axes both display maxima in September and minima in February and March, directly relating to the seasonal advance and retreat of sea ice over the year. The rotation angle of the major ellipse displays increased eastward rotation throughout much of the year, potentially representing the prevailing westerly winds around Antarctica causing advection of sea ice. The sharp rotation westwards during the summer is due to the sea ice breaking up and retreating towards its minimum rather than a change in the prevailing winds. The centroid coordinates display seasonal patterns as well, potentially representing a change in the centre of mass of the sea ice extent. However, the physical significance of the centroid of the ellipse has not been explored.

The ellipse parameter anomalies over the timespan of each dataset are seen in Figure 3.1b and these likewise show similar patterns across the three datasets. While there are small differences in both the parameters and anomalies between datasets, these are likely due to the differences in spatial and temporal resolution between them. The centroid coordinates for the QuikSCAT data between January and April do not match with the other datasets, but since the difference is still small compared with the range of coordinates, the differences only last for a small portion of the year and the standard deviations of all the datasets mostly overlap, this is not considered a major problem.

The statistical correlations between the parameters obtained from the three datasets can be calculated to ensure there is little or no bias between the datasets, and these are shown in Table 3.1.

The anomalies in the ellipse parameter data (Figure 3.1b) represent the long term periodicities and trends in the sea ice using elliptical diagnostics, presented here as fractional deviations from the mean value for each month. An obvious feature in the anomalies for the axes lengths and the rotation angle is the presence of clear structures, for example a period of consistent positive anomalies for axes lengths during 1991 and 1992 and a period of consistent negative anomalies in the rotation angle during 1987 and 1988. The anomalies for the total ellipse area are generally about the same magnitude as the anomalies for each of the axes, but there is little obvious structure. The centroid coordinates display the most fractional variation from their respective means, but little absolute deviation from the means since the ellipse centroids are always close to the South Pole. The anomalies in the rotation angle are large in terms of the fractional deviations form the mean. This suggests that the ellipse parameters highlight that the geographic distribution of the sea ice displays large variations on regional scales but the total integrated sea ice extent varies much less.

The absence of structure in the anomalies for the total ellipse area and presence of structure as well as greater anomaly magnitudes in the ellipse parameters suggest that while the total sea ice area is relatively insensitive to long term effects, there are geographic shifts in the sea ice cover. Changes in any one of the ellipse parameters naturally implies a change in the entire sea ice extent, so even if there is no significant change in total sea ice area the regional response to changes in atmospheric forcings can still be large. this is particularly apparent with the variations in the rotation angle of the major axis.

Table 3.1: Correlation coefficients for the parameters from each dataset. All correlations are ≫ 99% significance.

Ellipse Parameter	Hadley/ Bootstrap	Hadley/ QuikSCAT	Bootstrap/ QuikSCAT
Major axis	0.89	0.97	0.89
Minor axis	0.96	0.98	0.94
Rotation angle	0.86	0.97	0.90
Latitude	0.74	0.90	0.74
Longitude	0.74	0.88	0.78
Area	0.99	0.98	0.97

These long term effects can be analysed in terms of the dominant forms of interannual variability, namely the ENSO and SAM in this region, using several different methods, and conclusions can be drawn about how different atmospheric and oceanic circulation phenomena affect the Antarctic sea ice extent. The analyses presented here use the Multivariate ENSO Index (MEI, Wolter (1987); Wolter and Timlin (1993)) and the Marshall SAM index (SAM, Marshall (2003)).

Since the QuikSCAT data only last for five years, they were omitted from further analysis with respect to the ENSO and SAM. Only the Bootstrap and Hadley data were used for the
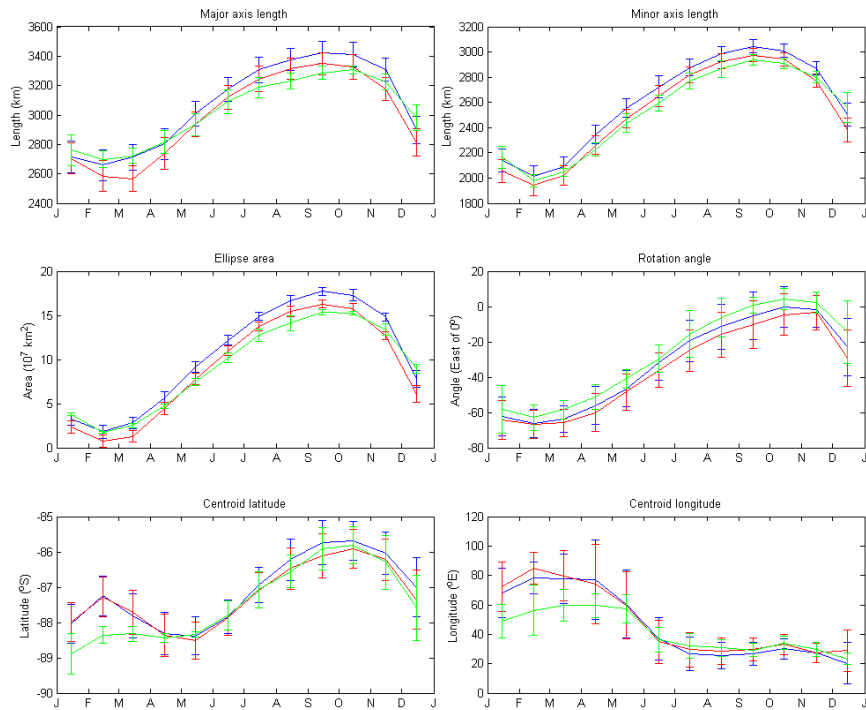
(a)
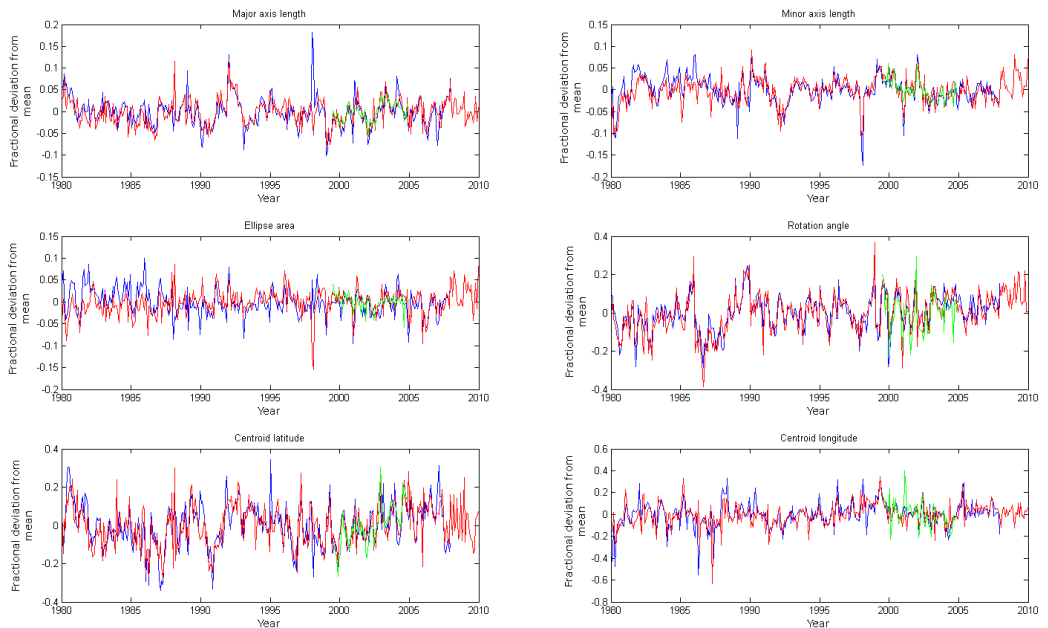
(b)

Figure 3.1: (a) Mean annual cycle in the ellipse parameters for the Hadley (red), Bootstrap (blue) and QuikSCAT (green) data. The bars in (a) represent the standard deviation in each parameter for each month. (b) Anomalies in each ellipse parameter, given as fractional deviations from the mean.

rest of the analysis due to their longer timespans.

While various analyses were able to be performed on the ellipse parameter data to examine the potential effects of ENSO and SAM on the Antarctic sea ice extent, much of the analysis is incomplete due to time restraints and several major disruptions to the research caused by the September 2010, February 2011 and June 2011 Christchurch earthquakes. As such, the results presented here in relation to the respective effects of ENSO and SAM on the Antarctic sea ice extent require further work.

3.2   Composite Analysis

The elliptical diagnostics allow the geographic spread of sea ice to be easily quantified. This quantification allows the effect of various atmospheric forcings on regional sea ice extents to be analysed in a different way to previous sea ice studies. Composite analysis is a technique where ellipses for extreme conditions are compared directly and the differing conditions associated with these extremes are analysed.

It was hypothesised that extreme ENSO and SAM events would significantly alter the geographic extent of Antarctic sea ice based on previous studies, namely Yuan and Martinson (2000, 2001) and Hall and Visbeck (2002). To examine this hypothesis, sets of ellipse parameters which produced large geographic displacements were found. Using a brute force search, for each month the two years which produced the largest geographic difference in sea ice extent were identified. Both the SAM and ENSO indices for those particular months as well as the previous six were examined to determine whether the differences could be related to the delayed effect of ENSO and/or SAM.

For two intersecting ellipses, the geographic shift in sea ice is calculated by subtracting the intersection of the two ellipse from their union. Figure 3.2 shows two intersecting ellipses representing two sea ice extents for the same month in different years, typical of the results presented here although exaggerated for clarity. The combination of the two ellipses A (blue) and B (red) can be split into five sectors (s_i) and the geographic difference between them calculated as follows:

$$
\begin{aligned}
\text{Shifted area} \quad &= \quad A \cup B - A \cap B \\
&= \quad (s_1 + s_2 + s_3 + s_4 + s_5) - (s_3) \\
&= \quad s_1 + s_2 + s_4 + s_5
\end{aligned}
\tag{3.1}
$$

In general, there is a consistent pattern of differing geographical distribution of sea ice with El Niño and La Niña events (Figure 3.5a and Figure 3.5b). There is also a change in the total sea ice area associated with differing ENSO events (Figure 3.5c). This change in total area appears in both the ellipse areas and the areas calculated directly from the satellite data. For the Hadley data, there is a similar magnitude of total sea ice change for both the ellipses and the observations, but for the Bootstrap data this change is different for ellipses during the winter (Figure 3.5). This is likely due to the different spatial and temporal resolution of the Bootstrap data causing minor changes to the area as calculated from ellipses.
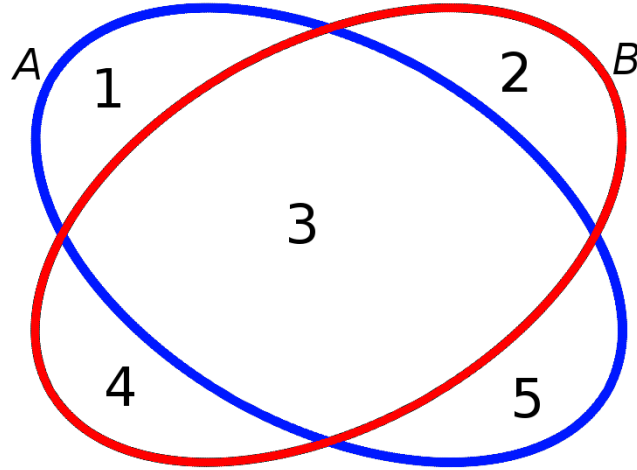
Figure 3.2: Schematic representation of how geographical shift in the sea ice is calculated. For ellipses A (blue) and B (red), the geographic shift in sea ice are is calculated as the difference between $A \cup B$ and $A \cap B$

The same analysis can be performed using the maximum change in rotation angle, which can be thought of as loosely relating to the prevailing winds. A positive (negative) rotation angle anomaly means that the ellipse is rotated further eastward (westward), suggesting increased westerly (easterly) winds. Since positive (negative) SAM is associated with strengthening westerlies (easterlies), it can be hypothesised that the rotation angle might have a correlation with the SAM. However, since the wind direction does not necessarily mean that the sea ice will shift in the same direction, care must be taken with this hypothesis.

3.2.1 Comparison with El Niño-Southern Oscillation

Examination shows that there are common responses to El Niño and La Niña events in this analysis, which are consistent with previous studies (Yuan and Martinson, 2001), namely that during El Niño events, there is a reduction in sea ice in the Ross Sea and an increase in sea ice in the Weddell Sea and these anomalies are reversed for La Niña events. The polarity of these anomalies reverses near the Antarctic Peninsula (Figure 3.3). It is notable that the ENSO index consistently remains in the same phase for most if not all of the six months preceding each ellipse shown here. This suggests that the large geographic shifts observed in the sea ice cover are the result of persistent El Niño or La Niña phases of the ENSO rather than isolated events. This observation is based purely on the results of the composite analysis performed here, so further analysis needs to be performed to verify these conclusions

The maximum geographic displacement of sea ice between any two years is very pronounced in January, February and March, with large positive anomalies in the Indian Ocean. These patterns are not realistic however, since the actual sea ice does not display these patterns in the summer months and instead is dominated by the Antarctic coastline. As explained in Chapter 2, the elliptical diagnostic technique is unrealistic and unreliable during

the summer months (December to March) due to the low sea ice areas at that time, so these results are questionable at best.

For most of the year, the largest anomalies occur in the Ross and Weddell seas, consistent with expected responses as described in Yuan and Martinson (2001). Little change is seen in the sea ice extent in the Indian and Pacific Ocean sectors for a large portion of the year. May and June display the largest positive anomalies in the Ross Sea during La Niña events, and this seems to be linked to the difference between moderate El Niño events and large La Niña events at 4-6 months lag. April and July have similar magnitude positive anomalies in the Weddell sea for El Niño events. For April the maximum geographic displacement from large El Niño occurs during moderate La Niña events, with sea ice patterns typical of such events. In July, the maximum displacement from large El Niño occurs not during La Niña, but during a weak El Niño event. However, this may not be representative of the July sea ice for La Niña events in general, since this analysis is just for the most extreme geographical displacements and not the general trends.

Apart from the minimum sea ice extent during the summer months, El Niño events from the Hadley data consistently produce increases in the total sea ice extent (Figure 3.5a). This increase is at a maximum between May and July where the sea ice extent can be over $1.5 \times 10^6 \text{km}^2$ greater than that during La Niña events. The increase in total sea ice area is apparent in the observational data as well, where similar patterns are observed. The magnitude of these areal changes vary somewhat between the ellipses and the observations, but this is likely due to how the ellipse areas are calculated compared to the observational areas.

The change in total sea ice extent between any two years during the maximum sea ice in September is negligible, although the largest geographic shift examined is almost $5 \times 10^6 \text{km}^2$. Since the geographic shift in sea ice extent between El Niño and La Niña events is consistently far larger than the change in total sea ice area, this shows that the ENSO has far larger effects on the sea ice extent at regional scales rather than hemispheric scales. Elliptical diagnostics are advantageous for this type of analysis since they allow this geographic shift to be quantified without requiring arbitrary sectors to be defined in the sea ice extent.

The largest change in total sea ice observed occurs during May, when there is a increase of almost $2 \times 10^6 \text{km}^2$. There is a large difference in the ENSO index for these two ellipses, but little difference in the SAM index. This suggests that the ENSO is at least partially associated with this change in total sea ice area.

3.2.2 Comparison with Southern Annular Mode

The response to the SAM using this analysis is far less conclusive. The SAM indices for the previous six months before each ellipse display little consistency in phase. This suggests that the regional response of the sea ice to SAM is insignificant compared to the response to the ENSO. However, since only these two external forcings are examined it is possible that while the magnitude of the SAM forcing is small compared to the ENSO forcing, it may still be a potentially important driver of sea ice extent variations. It is noteworthy that the ellipses for May and June from the Hadley data both display very positive SAM and large La Niña events coincident with large positive anomalies in the Ross Sea ice extent, consistent with

Stammerjohn et al. (2008). The Bootstrap data from May and June also show this, but with El Niño generally coincident with negative SAM phases as well. There is some evidence for opposite phases of ENSO and SAM coinciding to magnify the regional sea ice anomalies. Liu et al. (2004) has suggested that SAM and ENSO produce qualitatively opposite regional sea ice anomalies for the same phase, and this is partially supported by the composite analysis here. The analysis here shows that large El Niño events are often accompanied by SAM events of consistent negative phase and vice versa. However, this pattern is not particularly consistent in that it does not appear in every month, and even when it does it does not necessarily display consistently opposing trends between the ENSO and SAM phases.

There are no obvious patterns linking the rotation angle of the ellipse with the SAM index using this particular analysis. While it was hypothesised that positive SAM phases would increase the rotation angle eastwards due to the strengthening westerlies associated with positive SAM, no consistent link between the SAM and rotation angle is observed here. However, this analysis is incomplete in that the geographic shifts in sea ice due to purely the SAM or purely the ENSO are not examined, only the greatest geographic shifts between any two years are examined here.

3.3   Lag Correlation Analysis

In a similar analysis to Sen Gupta and England (2006), lag correlations between the ellipse parameters and the ENSO and SAM were performed on the anomalies from each dataset. For each ellipse parameter and dataset, correlations were calculated for zero to six month lags for both the SAM and ENSO in an attempt to identify the signature of each phenomenon on the Antarctic sea ice. The signature of these atmospheric phenomena have been detected previously in polar ice fields at varying lags (Yuan and Martinson, 2000, 2001) so it is not surprising that similar signatures are seen here. However, the way in which these signatures manifest themselves in the data is somewhat different to previous studies so further interpretation is needed to compare the results from each method. For example, Sen Gupta and England (2006) produce correlations between SAM and sea ice for each pixel of sea ice data, requiring analysis to interpret the results in terms of the total sea ice extent. Since changes in any one of the ellipse parameters analysed here alter the total sea ice extent, signatures of the ENSO or SAM manifesting in any one of the ellipse parameters naturally imply that their signatures manifest in the total sea ice extent as well.

Band structures are often seen in the lag correlation analysis. For example, the total ellipse area of the Hadley data displays a consistent correlation with the SAM (Figure 3.7b). At six months lag, this correlation is strongest in the September-October-November (SON) three-month period, and it is persistent until the synchronous correlation in the March-April-May (MAM) three-month period. This implies that the SAM has a significant effect on the total sea ice area for six months from MAM to SON. These patterns imply that the response of the sea ice to the SAM or ENSO can be delayed by up to several months, and in addition this response can be persistent for an extended period. This compares well with previous studies such as Sen Gupta and England (2006) and because these correlations exists in the various ellipse parameters, this allows the effect of SAM and ENSO on sea ice to be analysed
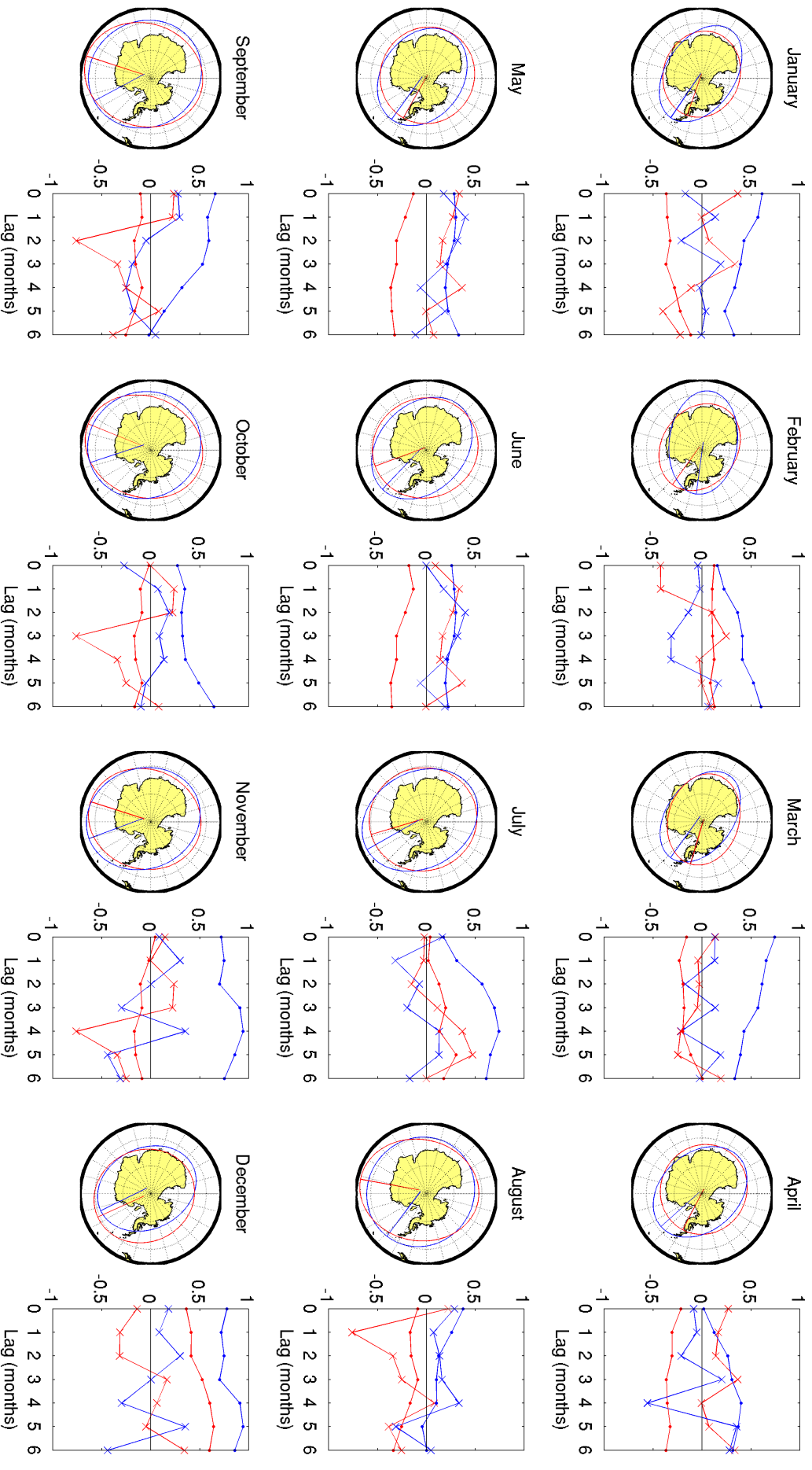
Figure 3.3: Maximum geographical displacement for each month from the Hadley data. The blue ellipse is the ellipse for the greater ENSO index and the red ellipse is for the lower ENSO index. The ENSO and SAM indices are displayed on the accompanying plots, normalised so that their intervals are $(-1, 1)$. Lags are displayed as well, from synchronous sea ice extent and SAM/ENSO index to SAM/ENSO leading the sea ice extent by six months. The colours correspond to the ellipses. Dotted data is for ENSO, crossed for SAM.
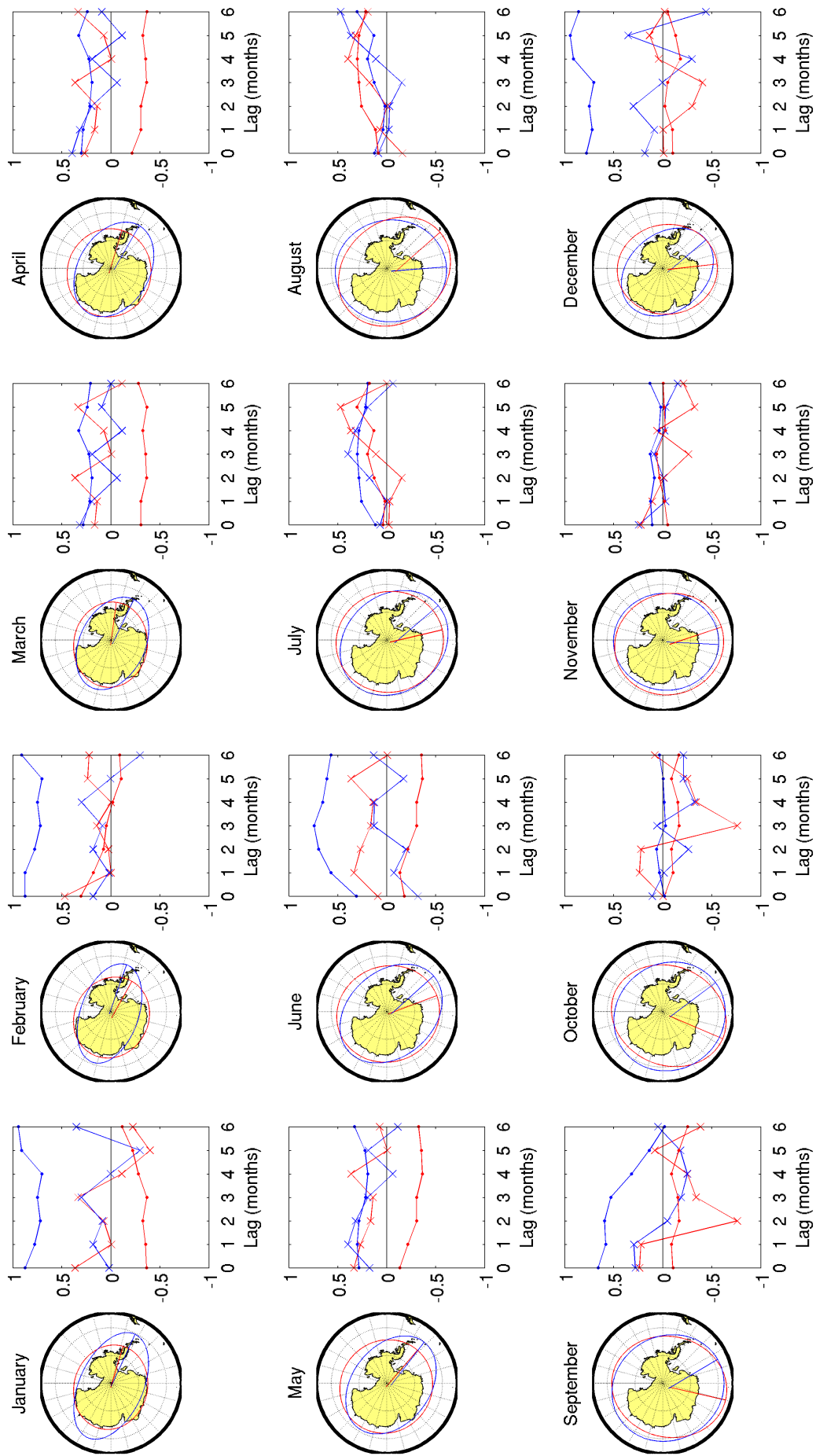
Figure 3.4: The same analysis as in Figure 3.3 but for the Bootstrap data.
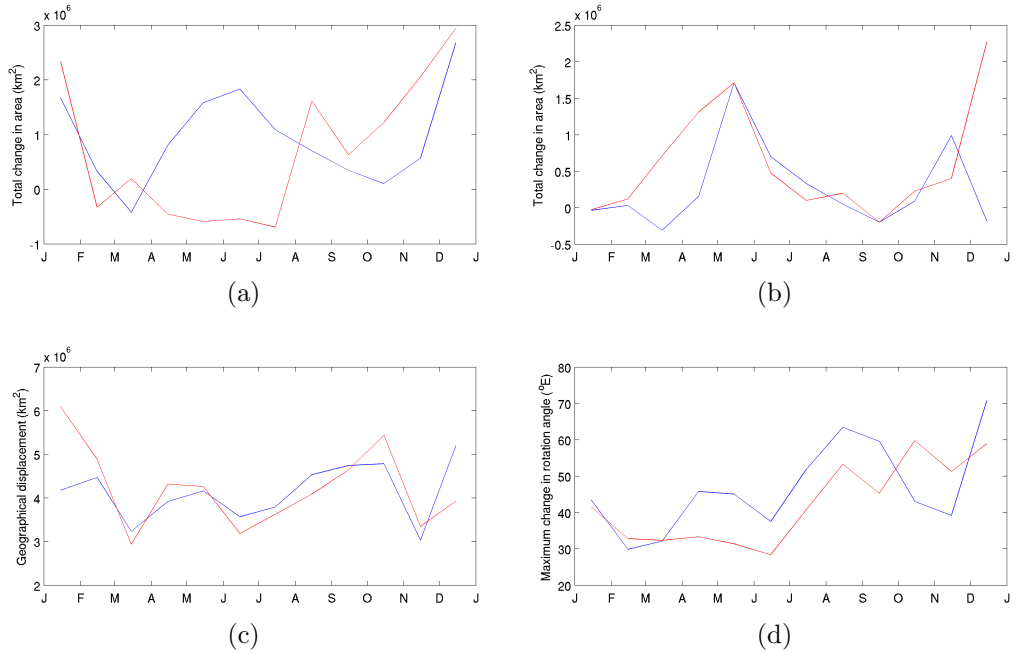
Figure 3.5: (a) Total area difference between El Niño and La Niña events from ellipses; (b) Total area difference between El Niño and La Niña events from observational data; (c) Geographical displacement of sea ice between El Niño and La Niña events; (d) Maximum change in rotation angle of ellipses for each month. For all plots, the blue data are for Hadley, red data are for Bootstrap.

in a way other than just that of total sea ice area and somewhat arbitrary regional sea ice extents.

3.3.1 Comparison with El Niño-Southern Oscillation

For the Hadley data, the most obvious correlation with the ENSO is that of the eccentricity of the ellipse (Figure 3.7a). This manifests as strong correlations from December to May which persist for several months, culminating in a strong positive correlation between the ENSO in January and the eccentricity in July. This correlation has the effect of increasing the sea ice extent in the Weddell Sea and reducing the sea ice extent in the Ross Sea during El Niño events. As seen in the composite analysis in Figure 3.3, the ellipses are indeed more eccentric during El Niño, which supports the conclusions reached in §3.2.

A similar although weaker band structure is seen in the rotation angle correlations, and this has a change in polarity during the late spring, coinciding with the rotation angle reversing as sea ice extent reduces to its minimum (Figure 3.7a). This reverse in ellipse rotation is typical of the ellipse behaviour for this period of the year (Figure 3.1a) but this is associated with the sea ice breaking up rather than a change in the prevailing direction of sea ice advection. This implies that El Niño phases of the ENSO slow the ellipse rotation during the latter half of the year. This seems to imply that El Niño decreases eastward sea ice advection as the sea ice reaches its maximum extent, and due to the nature of the sea ice during the summer minimum, the apparent rotation of the ellipse westward during the summer is slowed as well. This apparent westward rotation is attributed to the breaking up

of the winter sea ice extent so does not represent any significant change in the prevailing winds around Antarctica

There are no significant lag correlations seen in any of the other ellipse parameters, suggesting that the ENSO has little effect on the total sea ice area or the centroid of the ellipse, potentially representing the centre of mass of the sea ice.

3.3.2   Comparison with Southern Annular Mode

Stronger lag correlations are seen between the sea ice and the SAM rather than the sea ice and the ENSO, for both the Hadley and Bootstrap data. The most obvious correlation for both is for the latitude and longitude coordinates of the ellipse centroid. For the Bootstrap data, the latitude has a synchronous correlation in January and February and this remains significant for four months. The longitude only has a significant correlation with the SAM for between two and four months lag. While the latitude correlation for the Hadley data is small, only affecting one month for up to three months lag, the centroid longitude correlation is much more significant, affecting the longitude for a large portion of the year and at many months lag. The combination of these correlations suggests that positive SAM acts to rotate the ellipse centroid eastwards around the South Pole during the winter.

For the Bootstrap data, small negative correlations are seen in the total sea ice area, for both the ellipses and the actual data. These correlations only exist for greater than three months lag and only exist between December and March. These correlations suggest that large positive SAM in the early summer causes a minor decrease in sea ice area for the late summer, and since they show up in both the ellipse and data areas, they can be considered to be physically meaningful. In contrast to the Bootstrap data, there are extensive significant correlations for the Hadley data. Strong synchronous correlations are seen in May, and these are significant for the full six months lag, suggesting that the SAM has a large effect on the total sea ice area over the winter and continuing into the early summer. No negative correlations are seen in the same way as for the Bootstrap data, although this does not necessarily mean that those particular correlations are nonexistent, only that they are not statistically significant enough to show up in this particular analysis.

The Hadley data also shows moderately strong negative correlations for the eccentricity and rotation angle, here defined as westwards rotation. This suggests that the ellipses are more circular and rotated further eastwards with positive SAM. Since this eastward rotation can be loosely thought of as relating to the increase in prevailing westerly winds associated with positive SAM, this supports previous studies relating changes in sea ice to the SAM (Liu et al., 2004). Combined with the positive correlations for area, this suggests that the sea ice displays opposite area anomalies between SAM phases, and in addition these anomalies are larger for positive SAM.

The lag correlation analysis for the SAM and ENSO show opposite results to the composite analysis examining the factors causing large geographic shifts in the sea ice cover. While the composite analysis suggests that the ENSO signal is dominant in controlling the geographic distribution of the sea ice, the lag correlation analysis shows that the SAM is dominant mode of atmospheric forcing of Antarctic sea ice. However, the lag correlation analysis does not take into account the magnitude of the changes caused by each respective

circulation mode, only the consistency of these changes. The lag correlation analysis therefore suggests that while the magnitude of the changes in sea ice cover caused by the SAM are relatively small compared to those caused by the ENSO, they are more consistent.

The composite analysis does not take into account the consistency of the changes caused by the two circulation modes studied here, it only examines the largest geographic shift between sea ice extents for any two years. Since the ENSO appears to be the dominant factor in the geographic shifts as examined here, this suggests that the magnitude of the changes in the sea ice cover caused by the ENSO can be larger than those of the SAM, but they are not as consistent.
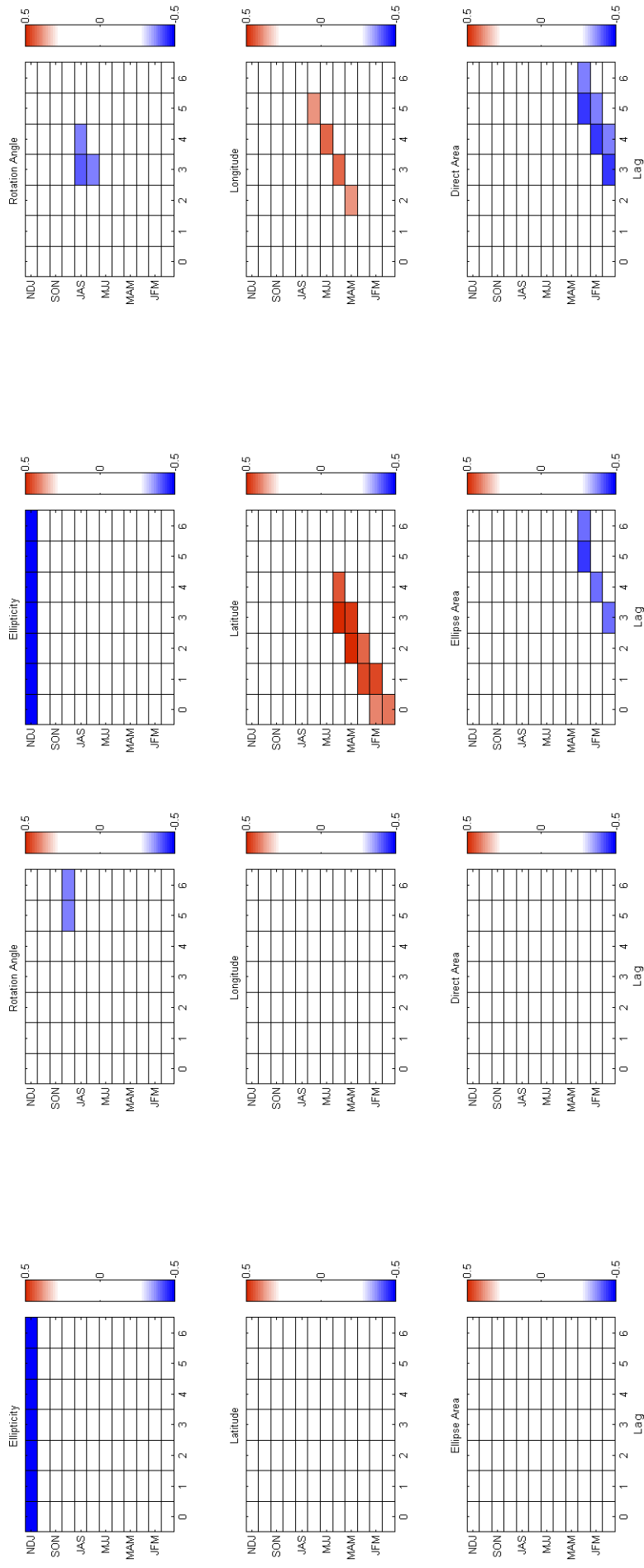
Figure 3.6: Lag correlations for (a) Bootstrap and ENSO; (b) Bootstrap and SAM for 0-6 months lag for running three-month intervals. Positive lag corresponds to the ENSO/SAM leading the sea ice. Only correlations with $\geq 95\%$ confidence are shown.

Figure 3.7: Lag correlations for (a) Hadley and ENSO; (b) Hadley and SAM for running three-month intervals. Positive lag corresponds to the ENSO/SAM leading the sea ice. Only correlations with ≥ 95% confidence are shown.

3.4 Empirical Orthogonal Functions

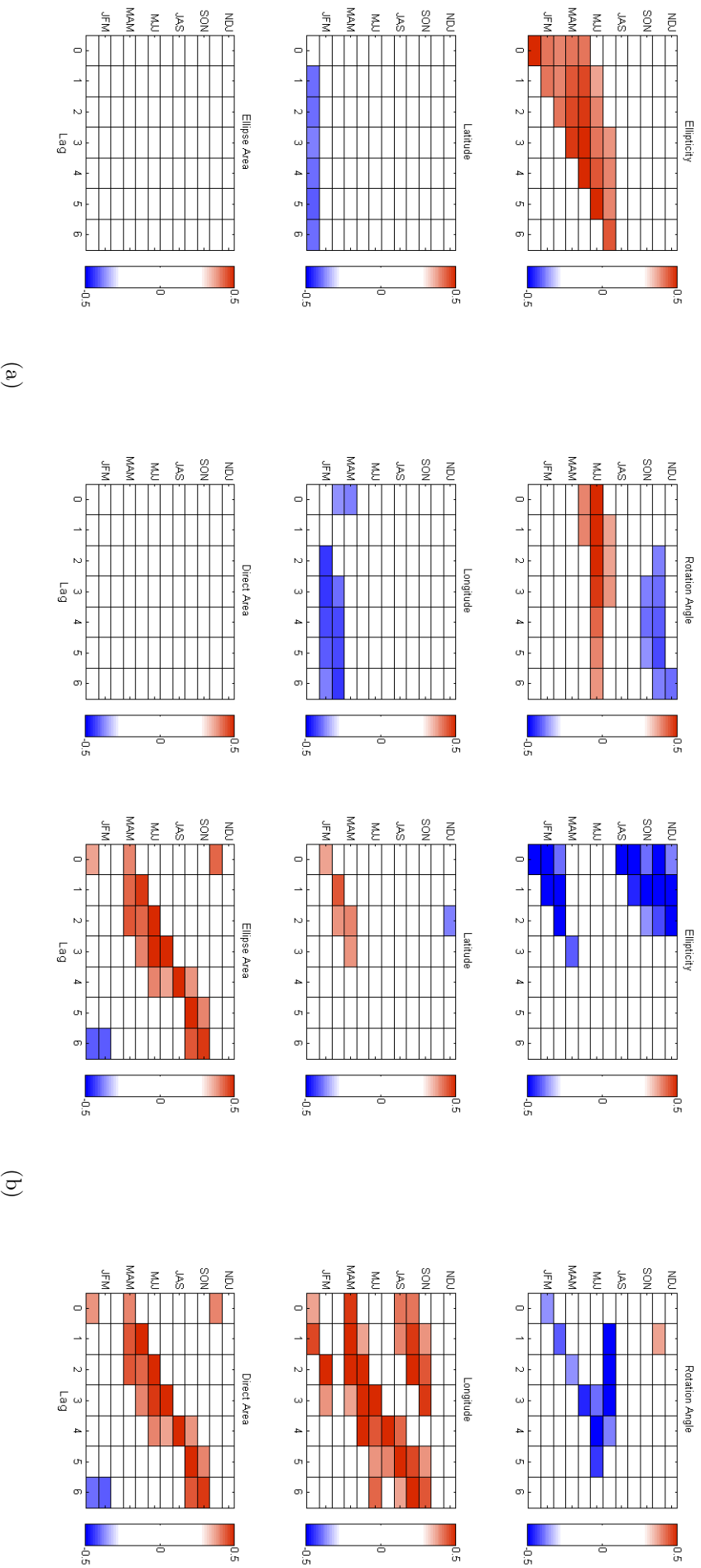A common method of exploring geophysical data is to perform a principal component analysis (PCA). When weighted geographically, the PCAs are known as empirical orthogonal functions (EOFs), so the analysis provides a set of basis functions for explaining the spatial and temporal variations in the data. The advantage of EOF analysis is that complex physical data can be compressed into a few spatially and temporally orthogonal and hence uncorrelated functions which represent most of the variance in the physical data. This technique is purely statistical however, so the EOF modes produced may not have any physical significance. Despite this potential drawback, EOF analysis has been used extensively in previous sea ice studies, for example Yuan and Martinson (2001) and Sen Gupta and England (2006).

Using a method similar to Yuan and Martinson (2001), the EOFs for the anomalies in the sea ice edge as provided by the ellipse fitting can be extracted from the data and analysed. Using the ellipse parameters fitted to the sea ice for each timestep, a set of latitude and longitude coordinates approximating the sea ice edge were found. The anomalies in the sea ice edge are then determined by taking the latitude anomaly for each longitude coordinate. The anomalies are then passed through a low-pass filter to remove any periodicities in the data of less than one year. This allows solely the long-term trends in the EOFs of the sea ice edge to be analysed.

Since the ice edge is broken up into 360 sectors of 1°longitude each, the EOF analysis provides a set of 360 basis functions, or modes, to describe the sea ice edge at each longitude point. For the Hadley and Bootstrap data, the fist two EOF modes together describe 94% of the variance in the sea ice edge anomalies. The first two EOF modes for the QuikSCAT data describe 97% of the variance. These are remarkably high, but they are likely due to the simplification of the sea ice edge position when using ellipses. For an ellipse, two different EOF spatial patterns rotated by 90° could potentially explain most of the variation seen in the simplified ice edge as the magnitude of each pattern changes. A similar analysis was performed to analyse wavenumber two behaviour in the Antarctic sea ice by Udagawa et al. (2009).

The eigenvectors of the two leading EOF modes in the sea ice edge anomalies of each dataset show clear peaks at about 20°E and 160-180°W and troughs at about 80-100°E and 80°W (Figure 3.8). The largest peak is at 160-180°W and this is in a similar place to the Antarctic Dipole as shown in Yuan and Martinson (2001). This peak is not in the exact same location, but since the ellipses are far more regular than the actual sea ice extent this is not surprising as the ellipses do not necessarily pick up all the localised irregularities in the sea ice associated with the ADP.

The sea ice anomalies were reconstructed from the leading EOF modes to examine the long period variations in the sea ice. Firstly, the EOF time series were low-pass filtered to remove any interannual periodicities since these periodicities dominate the variations in the sea ice anomalies. The resultant time series show a clear standing wave pattern in the sea ice which corresponds well to the ADP (Figure 3.9). There are consistent peaks of opposite sign at about 250°E and 330 °E, signifying an out of phase relationship in sea ice extent over the Antarctic Peninsula. This relationship also implies a similar out of phase relationship of opposite sign in Antarctic surface temperatures over the Antarctic Peninsula, and this
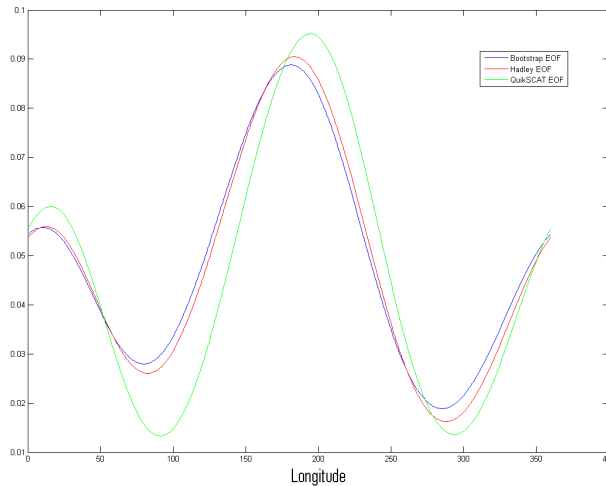
Figure 3.8: The integrated eigenvectors of the first two EOF modes of the sea ice edge anomalies as functions of longitude for the Bootstrap (blue), Hadley (red) and QuikSCAT (green) data.

agrees well with analysis in Harangozo (2000) and Comiso (2000). As examined in Yuan and Martinson (2001), there are large positive phases of the ADP in 1979, 1992 and 1995 and large negative phases in 1986, 1988 and 1990. The sea ice anomalies as reconstructed here produce these particular extrema with limited success, however the same general patterns appear. Some of the large peaks in the EOF reconstructions loosely coincide with ENSO events, for example the large El Niño events in 1992 and 1998 and the large La Niña event in 1989.

This analysis displays limited evidence for a travelling wave in the Antarctic sea ice, corresponding to the ACW. Between 2001 and 2005, there is a consistent eastward rotation of the extrema in the sea ice edge anomaly. Between 1986 and 1988 a similar pattern appears, but this time displaying a westwards rotation. Since these patterns show opposite behaviour and are not persistent over more than a few years, they cannot be considered evidence for the ACW, and this is supported by Park et al. (2004).

Although the EOF analysis displays some evidence for a standing wave structure in the Antarctic sea ice using elliptical diagnostics which may be related to the ENSO, it is incomplete and hence speculative. In particular, the physical significance of the leading EOF modes remains unclear, and since the EOF analysis technique is purely statistical, there may not be any physical significance in the leading EOF modes.
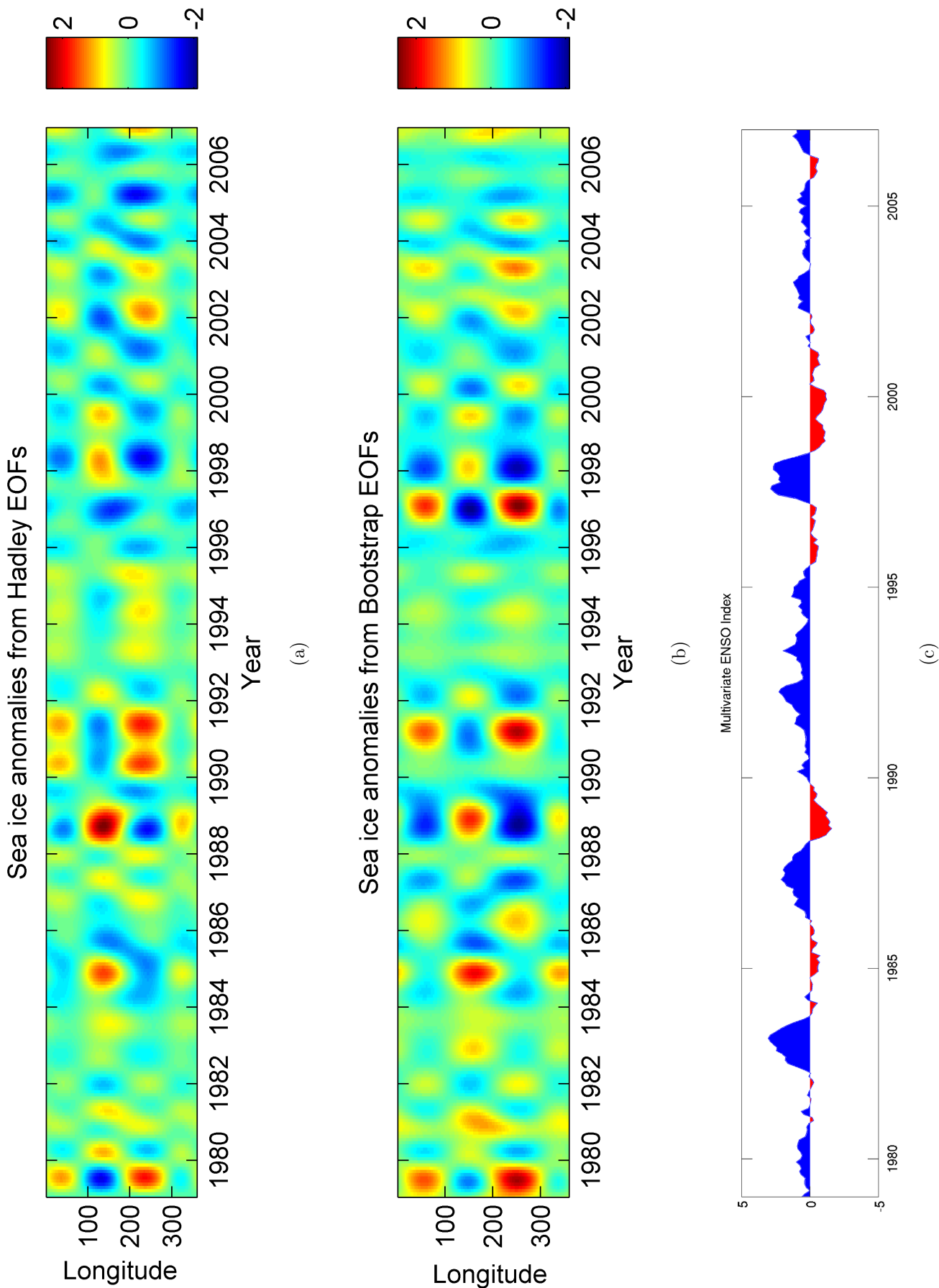
Figure 3.9: Sea ice anomalies as reconstructed from the two leading EOFs of the Hadley (a) and Bootstrap (b) data. (c) The ENSO is displayed for the same time period for comparison purposes, with positive phases of ENSO shaded blue and negative phases shaded red. The QuikSCAT EOFs are not shown here since they only run for five years, not 28.

Chapter 4

A Method for In Situ Sea Ice Measurement - SNOW-WEB

This chapter details a new method for measuring small-scale atmospheric conditions and their potential effects on the Antarctic sea ice extent. The development of the first generation of the SNOW-WEB network and its deployment between Scott Base and Windless Bight during January 2011 in Antarctica is described here as well as the initial results from these field trials.

4.1 Summary of the SNOW-WEB project

The SNOW-WEB project is a long term project undertaken by the atmospheric physics research group at the University of Canterbury. Its goal is to develop a network of weather stations that communicate wirelessly in order to monitor atmospheric conditions at very high spatial and temporal resolution over extended periods in harsh environmental conditions such as those encountered in Antarctica. One of the intended uses of the SNOW-WEB system is to measure surface winds around the edge of the Ross Ice Shelf with the particular goal of verifying the conclusions drawn about increased southerly winds in the Ross Sea and their influence on sea ice detailed in Turner et al. (2009). Turner et al. (2009) shows that since 1979, an increase in transport of ice out of the Ross Sea during the autumn is caused by southerly near-surface winds increasing. This increase in southerly winds gives rise to lower air temperatures, helping to maintain the polynyas along the coast of the Ross Sea and hence increasing ice production and promoting increased northwards ice advection. Developing a method of in situ measurement to understand the details of the winds that likely affect sea ice is important to verify the conclusions drawn in Turner et al. (2009).

The high temporal and spatial resolution of SNOW-WEB allows detailed measurements to be taken of atmospheric phenomena and how they respond and evolve over time. An example of this is examining how a temperature front might propagate over a certain area and react to the local topography.

The wireless communication capability of the stations (nodes) allows the status of the entire network to be monitored from any individual node in real time, and this capability also allows the network to function even if some nodes are inoperative. This is an advantage

over traditional automatic weather stations (AWS) which require manual retrieval of stored data. Also, since AWS systems are generally deployed alone, they are useless if they break down or are otherwise rendered inoperative. The redundancy inherent to the SNOW-WEB system potentially overcomes this limitation.

For the Antarctic field campaign in January 2011, the first generation of SNOW-WEB was deployed and tested on the Ross Ice Shelf in Antarctica. SNOW-WEB nodes were set up spanning a length of about 25km from Scott Base to Windless Bight.

4.2   SNOW-WEB node components

The core of each node was a circuit board with the following components attached:

- **AVR Mega64 Microcontroller (Atm, a):** This is the core component of each node. The microcontroller processes the signals from each instrument and either stores the data in its onboard 64kB memory or sends it to the XBee/XBeePro transceiver using the RS232 serial communication protocol. The data can also be transferred into the flash memory card for long-term storage. The nodes are also equipped with a 9-pin RS232 port to allow external monitoring of the SNOW-WEB network using a laptop computer and serial cable. The microcontroller also interprets signals received from other nodes and takes appropriate action if necessary, for example synchronisation of the onboard clock with an external reference.

- **Copernicus II GPS Receiver (Tri):** The acquisition of a GPS signal allows the position of each node to be known and an accurate time reference to be kept. Due to the cold conditions in Antarctica, the onboard oscillators keeping time on the microcontroller and real-time clock have the potential to become inaccurate over time, causing discrepancies when comparing timestamps from different nodes. This could cause significant issues if a GPS time reference was not available. The GPS also allows differential measurements to be taken between nodes, providing the potential for SNOW-WEB to be used to measure movement rates of sea ice and the ice shelf.

- **NXP PCF8583 real time clock (NXP):** Since this clock has a much lower power consumption rate than the microcontroller and GPS receiver (Table 4.1), it is used for most of the timekeeping functions in the node since it can be active constantly. Periodic synchronisations with the GPS signal are required to ensure the clocks accuracy.

- **Atmel Data Flash card (Atm, b):** This component provides 8MB of non-volatile memory for long term data storage of weather measurements.

- **Maxstream XBee/XBeePro wireless transceiver (Dig):** The transceiver is a RF communication device that operates in the ISM band of 2.4GHz. It meets the IEEE 802.15.4 standard for low-power wireless communications devices and has a RF data rate of 250 kbps. The communication between transceivers is serial and half-duplex, so the modules may only be transmitting or receiving at any one time, not both. The XBee module is the basic version, with a maximum transmitting power of 1mW and

and receiver sensitivity of -92dBm. The XBeePro is a higher-powered version of the XBee module, with a maximum transmitting power of 100mW and a receiver sensitivity of -100dBm. The XBeePro module was used in the SNOW-WEB nodes deployed in Antarctica. The next generation of the system will use ZigBee enabled XBee/XBeePro modules for full mesh networking.

- **Isotropic half-wavelength whip antennae (Jin):** To facilitate line-of-sight communication between the nodes, antennae with a measured gain of 13 dBi, operating frequency of 2.4 GHz and a bandwidth of 83 MHz were fitted to the nodes and mounted at either 2m or 4m height. While the XBee/XBeePro modules can be fitted with on-board antennae, the inclusion of the large whip antennae increase the communication range between nodes to well over 10km in good conditions. This style of antennae was chosen due to their low cost and bulk, and the fact that they do not require alignment with other antennae to send and receive wireless signals at acceptable strengths. Using directional antennae such as Yagi antennae would provide the SNOW-WEB nodes with a greater communication range and stronger signal strength for the same power usage, however issues with aligning the antennae to enable sufficient signal strength for communicaton prevented their use in Antarctica. Their increased bulk and cost compared to isotropic whip antennae were other factors preventing their use in the field.

- **12V 9Ah Sealed lead acid battery (Dia, b) and solar panels (Soa):** The nodes were powered with a sealed lead acid battery rated at 9Ah. This type of battery was used due to its large capacity and insensitivity to the cold compared to smaller AA sized batteries. To keep the batteries from draining, a pair of small 12V solar panels rated at 5W each were fitted to each node. They faced in opposite directions in order to gather as much sunlight as possible. Since the sun is above the horizon for 24 hours in the Antarctic summer and a lot of sunlight is reflected off snow, this proved to be a very efficient way to power the SNOW-WEB and keep the batteries charged. This system exceeded performance expectations because of the constant solar charging, and this means a major limiting factor, namely power consumption, is an issue of much less concern in the next generation SNOW-WEB design.

- **Sensirion SHT75 Humidity and Temperature Sensor (Sen):** This is a small (19.5×5.08mm) solid state relative humidity and temperature sensor. Humidity is measured using a capacitive sensor element and temperature is measured using a band-gap sensor. The low power consumption and small size are ideal for use in the SNOW-WEB nodes.

- **VTI Industries SCP1000-D01 Pressure sensor (VTI):** This is a capacitive sensor that measures absolute pressure. It was chosen due to its small size, low cost and low power consumption.

- **NRG #40H Cup anemometer (NRG):** Traditional cup anemometers were used to measure the wind speed due to their low cost and power consumption compared to more advanced instruments like ultrasonic anemometers. A disadvantage of this

system is that since it uses moving parts, it is susceptible to freezing up due to snow and ice buildup. For the limited time for which the SNOW-WEB was deployed in the Antarctic summer, this proved not to be a problem.

- **NexGen Wind #200P Wind vane (Nex):** The wind direction was measured using a traditional style wind vane, again due to their low cost and power consumption. They are susceptible to freezing up like the cup anemometers since they employ moving parts.

Except for the actual instruments, solar panels and antennae, all the components were mounted in plastic boxes lined with high-density foam for insulation. This proved to be an effective way of keeping the components from becoming too cold to function properly.

4.3 Battery life testing

One of the most important components of the SNOW-WEB was a power supply that would withstand the harsh Antarctic environment for several weeks continuously. Different power supply mechanisms were tested by setting up a SNOW-WEB circuit board with each power supply inside a freezer and allowing the assembly to run until the power supply could no longer run the SNOW-WEB board. All the electronic components of the SNOW-WEB circuit board are rated to operate in at least -40°C, but since the batteries used drain quickly in the cold, the performance of the equipment when insulated was tested as well.

One of the aims of the testing was to reduce the power consumption of the instruments so that a 12V lead acid battery rated at 7Ah could power the node for a week on a single charge, necessitating the daily power consumption of the instruments to be no more than 1Ah. This power consumption issue also determined whether certain components could be run continuously or had to be put into low power sleep modes occasionally during routine operation.

Using the current draw specifications for each instrument (Table 4.1), a power consumption scenario was designed for the node that would use less than 1Ah per day while taking measurements and communicating with the rest of the SNOW-WEB network every two minutes. Since the GPS receiver and the XBee/XBeePro transceivers use the most power, the scenario was designed to use these components as sparingly as possible. After activation, the GPS requires approximately 20-30 seconds to acquire a signal, so this was activated first along with the microcontroller. The wind velocity, temperature, pressure and relative humidity measurements were taken and then stored in the onboard flash memory. The transceiver was active for only a short time, and most of this time was spent listening for communications from the network. The scenario used for testing is described in Table 4.2, and this scenario uses a total of 0.92Ah per day.

The RM Young ultrasonic anemometer was not used in the SNOW-WEB nodes, but since the anemometer and wind vane used to measure the wind velocities use less power together than the ultrasonic anemometer, the power consumption scenario in Table 4.2 is still valid.

The nine tests performed on the SNOW-WEB node and its power supply are summarised in Table 4.3. The initial three tests were performed with AA size nickel-metal hydride batteries and were simply to ensure that the test node and all connected instruments and

Table 4.1: Current draws for each operating mode of each component used in the SNOW-WEB nodes.

Component	Current Draw (mA)			
	Sleep	Idle	Active/Transmit	Recieve
XBee	0.01	50	45	50
XBeePro	0.01	55	215	55
Microcontroller	0.001	12	20	-
PCF8583 clock	0	0.05	0.2	-
SHT75 sensor	0.001	0	5.5×10^{-4}	-
Copernicus II GPS	0	0	40	-
Flash memory	0.025	0	15	-
RM Young Anemometer	0	0.32	12	-
RM Young Temperature probe	0	0	5	-

Table 4.2: Power consumption scenario used for testing the SNOW-WEB nodes.

Component	Time active per two minute cycle (s)				Total power consumption (Ah)
	Sleep	Idle	Active/Transmit	Recieve	
XBeePro	105	0	5	10	0.312
Microcontroller	90	0	30	-	0.12
PCF8583 clock	0	0	120	-	0.0048
SHT75 sensor	105	0	15	-	2.27×10^{-5}
Copernicus II GPS	90	0	30	-	0.24
Flash memory	105	0	15	-	0.046
RM Young Anemometer	0	90	30	-	0.078
RM Young Temperature probe	0	0	120	-	0.12
Total power usage (Ah)					0.92

components functioned correctly. AA batteries were briefly considered as a possible power supply, but their low energy capacity and susceptibility to cold prevented their use in the field.

The fourth test was the first one with the test node mounted in a freezer and the first one using a sealed lead acid battery for the power supply. Since this test outlasted the AA battery tests by almost a factor of three, the sealed lead-acid battery was determined to be the ideal power supply for field testing of the SNOW-WEB network. Solar charging was tested as a means to prevent the battery from running out of charge, and these tests were very successful, culminating in the eighth test where the node ran successfully for ten days with no appreciable drop in battery voltage during the day. However, there were issues with the battery running out of charge during the night, but since the daytime performance was quite good, this was not considered to be a problem because of the constant sunlight in Antarctica.

The insulation used for the power tests was a thick polystyrene box, used in the sixth through ninth tests. Since polystyrene is a restricted material for Antarctic deployment, this was not used for the actual SNOW-WEB, but high-density foam was decided to be a suitable substitute. The heat from the battery and circuits kept the contents of the box about 9°C warmer than the surrounding freezer. Using a resistive heating circuit powered using an external power supply increased this temperature difference to 20-25°C, effectively preventing the battery and circuit board from dropping below 0°C. However, a resistive heating circuit is a large drain on power so was not included in the SNOW-WEB design. This circuit proved unnecessary in the final design since the SNOW-WEB electronics box was subject to ample solar radiation in Antarctica and this warmed the contents of the box significantly. All the testing was done in a sealed, dark freezer so this was not apparent during testing.

For all the tests, a laptop was connected to the circuit board through the board's onboard serial port. The output of the board through the serial port could be read and stored as a plain text file, allowing the measurements acquired during the power testing to be recorded and examined. This output was in ASCII text format displaying a timestamp, battery voltage, weather measurements and a GPS string. While the measurements themselves were irrelevant to the power testing, the length of time for which they ran was important, especially because they would become incoherent when the battery voltage passed a critical threshold, providing a means to determine a minimum voltage for which the SNOW-WEB nodes would run reliably, namely 4.0-4.1V. The length of time recorded for each test in Table 4.3 is the time between the start of the test and the time for which the last coherent data string was acquired.

4.4 Design and testing of research-grade weather station

To provide reference measurements to calibrate the SNOW-WEB nodes, a research-grade weather station built using commercially available components was designed and assembled at the Antarctic base camp beside one of the SNOW-WEB nodes. Since this station has been

Table 4.3: Summary of the nine power tests performed on the SNOW-WEB.

	Power source	Transceiver	Duration	Purpose
1	4 AA NiMH Batteries	XBeePro	20 hours	Initial test to ensure all components function correctly
2	4×AA	XBeePro	18 hours	First test with all components running continuously
3	4×AA	XBee	21 hours	As for (2), but using the XBee instead of the XBeePro
4	6V Lead Acid Battery	XBee	55 hours	First test using sealed lead acid batteries with the entire assembly placed in a freezer, uninsulated
5	6V Battery and solar charger	XBee	3 days	First test using a solar trickle charger as well. Only the battery was insulated.
6	6V Battery and solar charger	XBee	27 hours	First test with the entire assembly insulated to see how well the insulation performed.
7	6V Battery and solar charger	XBee	48 hours	Test with an externally powered heating circuit as well as insulation.
8	6V Battery and solar charger	XBeePro	10 days	Long term test without heating circuit
9	6V Battery and solar charger	XBeePro	4 days	Second long term test as for (8). This test was interrupted after four days by the September 4 earthquake in Christchurch.
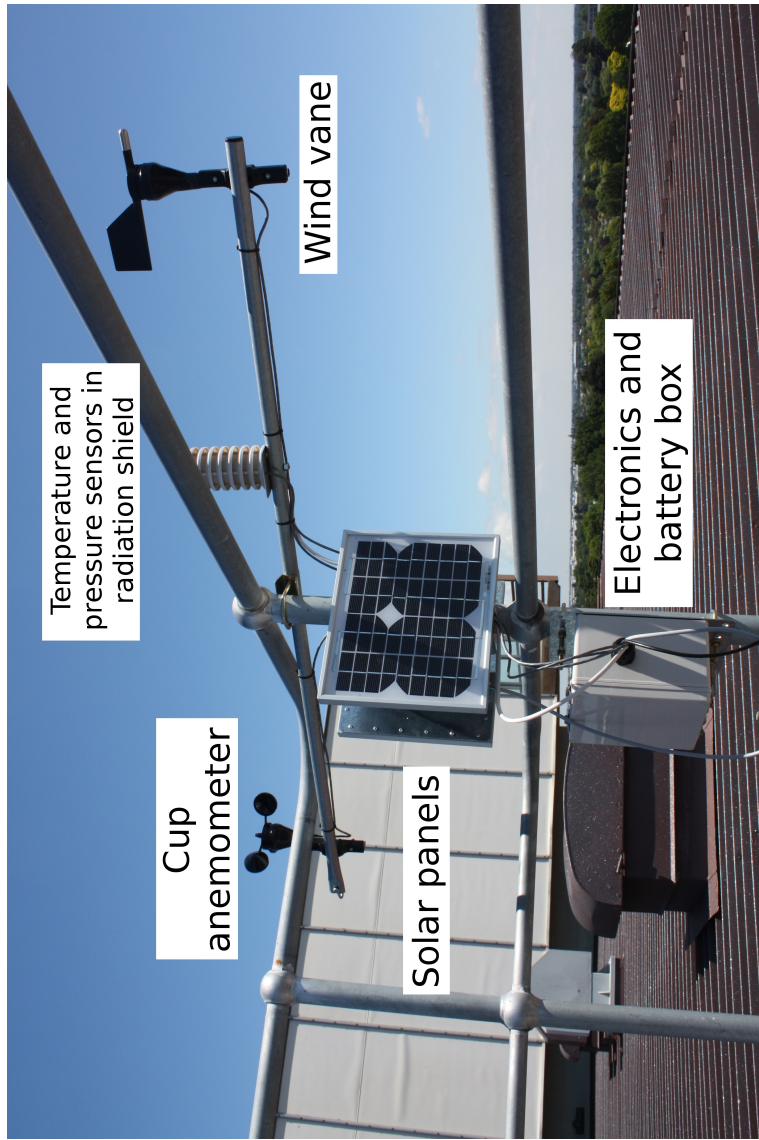
(a)
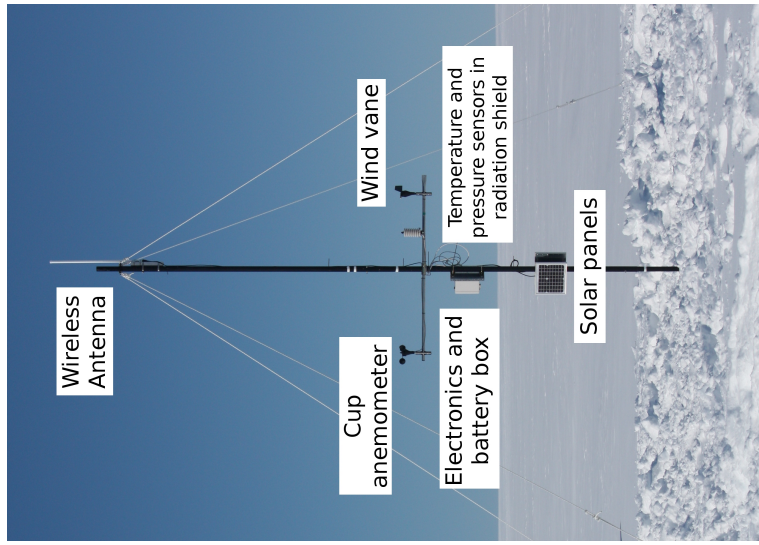
(b)

Figure 4.1: (a) SNOW-WEB node set up for testing on top of the Rutherford Building in Christchurch. (b) typical SNOW-WEB node deployed in Antarctica.

tested to ensure it is accurate in all its measurements, it provides an ideal reference baseline for the SNOW-WEB. Its location coincident with a SNOW-WEB node ensured that the atmospheric conditions would have negligible differences between the two weather stations.

4.4.1 Components

- **Campbell Scientific CR1000 Datalogger (Cam, a):** This was the control unit for the weather station. It can be programmed to record measurements from up to 16 different instruments at arbitrary intervals and store this data in its 4MB onboard memory. For the five instruments used here, the memory can last for over 100 days when taking measurements every ten minutes. The datalogger has no wireless capability so the data stored on it must be retrieved manually. The datalogger was mounted in a weatherproof enclosure which could be heated.

- **12V 40Ah lead acid batteries (Dia, a) and BP 380 80W solar panel (BP):** The weather station was powered by a set of four 12V sealed lead acid batteries similar to car batteries rated at 40Ah mounted in an insulated box. The batteries were on a constant charge using a 1209×537mm sized solar panel oriented northwards to gather the most sunlight. This arrangement provided ample power for the weather station in the 24 hour sunlight of the Antarctic summer.

- **Triangular lattice mast:** The entire weather station was mounted on a 6m high mast which was guyed and connected to a plywood base buried in snow for stability.

- **RM Young 41342VC Temperature Probe (R. , b):** Two temperature probes were mounted on the weather station at heights of 2m and 6m above the ground. These probes employ a platinum thermocouple which responds linearly to changes in temperature from -50°C to +50°C.

- **RM Young 41003 Multi-Plate Radiation Shield (R. , a):** The temperature probes were mounted in radiation shields to prevent errors in temperature measurements from sources such as solar radiation, precipitation and wind.

- **RM Young 85004 Ultrasonic Anemometer (R. , c):** The wind velocities at the weather station were measured using an ultrasonic anemometer rather than the traditional setup of a cup type anemometer and a wind vane. The anemometer has two sets of transducers aligned perpendicular to each other and the wind velocity can be determined by measuring the flight time of sonic pulses between these transducers. Ultrasonic anemometers have no moving parts so are suitable for deployment in Antarctica where traditional anemometers can be affected by snow and ice buildup. This style of anemometer was desirable for use on the SNOW-WEB nodes, but power consumption issues prevented this.

- **Campbell Scientific SR50A Sonic Ranging Sensor (Cam, b):** The accumulation of snow at the base of the weather station was measured with this instrument. This instrument works by sending out ultrasonic pulses and measuring the return time to determine a distance to the surface below it. Since the speed of sound in air is

proportional to temperature, the measurements are corrected with the temperature at the time of measurement to ensure accurate distance readings.

- **Vaisala PTB210 Digital Barometer (Vai, a)/ Vaisala SPH20 Static Pressure Head (Vai, b):** The atmospheric pressure was measured using a barometer in a weatherproof casing mounted on a static pressure head to minimise errors in pressure measurements from wind. The static pressure head used can be heated in order to prevent ice and snow buildup from blocking the pressure sensor.

4.4.2 Weather station testing

To test the accuracy of the instruments and the capabilities of the power supply used, the weather station was set up on the roof of the Rutherford Building at the University of Canterbury and allowed to run for an extended period of time (Figure 4.2a). The measurements obtained from the station were compared with the weather measurements from a similar station located on top of the Geography building at the University. This weather station was assumed to be accurate and was located within several dozen metres and at a similar altitude to our system.

The comparison between the reference weather station and the Geography weather station are shown in Figure 4.3. The Geography weather station records at ten minute intervals while the reference station records at 30 second intervals. Ten minute means of the reference station data are shown here for comparison purposes. The temperature measurements are almost identical as seen in Figure 4.3a and the wind velocity measurements are also relatively consistent. Due to the turbulence produced by the building's structure, the wind speed and direction for the Rutherford weather station vary a lot and are not always concordant with the Geography weather station, but still display reasonably similar patterns to the Geography weather station as seen in Figures 4.3b and 4.3c. Despite minor discrepancies with the Geography weather station data due to slightly different ambient conditions, the consistency of the measurements with known reference values suggests that the weather station performs with sufficient accuracy for use as a calibration station for the SNOW-WEB.

4.5   Results from Antarctic fieldwork

The Antarctic field campaign ran for three weeks from the 10th to the 31st of January 2011. Ten SNOW-WEB nodes were deployed over an approximately 25km span from Scott Base to Windless Bight (Figure 4.5), and the reference weather station was deployed at base camp beside a SNOW-WEB node, approximately 20km from Scott Base. While problems were encountered with the wireless communication between nodes which hindered the data retrieved, the hardware and power supplies of the nodes performed well in excess of expectations. A subset of nodes were configured to become backup data logging nodes, and the data became more continuous. In addition, the reference weather station logged data without issues for eight days from the 20th to the 28th of January.
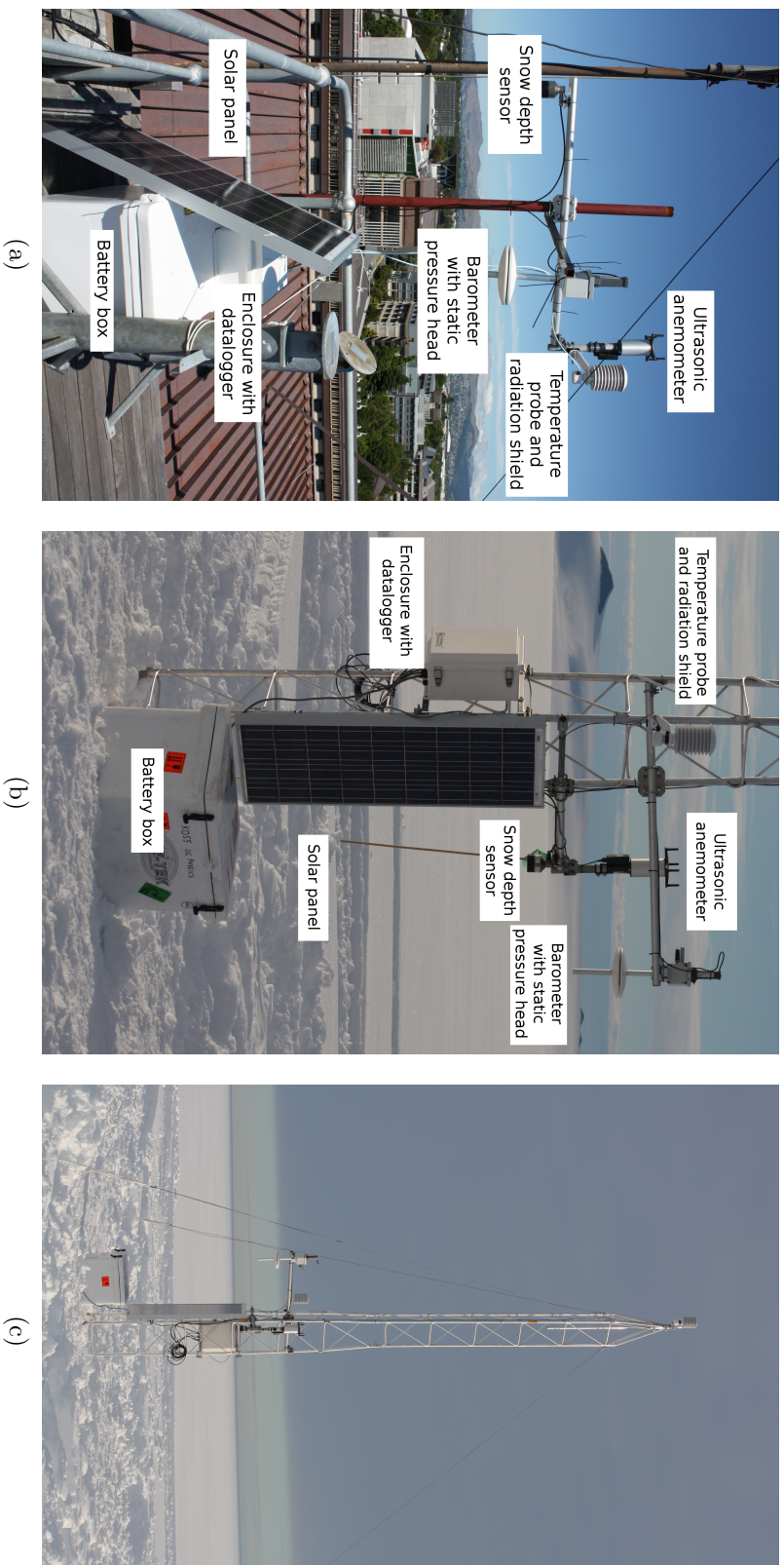
Figure 4.2: (a) The instruments of research-grade weather station set up for testing on top of the Rutherford Building in Christchurch. (b)(c) The weather station as deployed in Antarctica. (b) shows the components at the base of the tower, (c) shows the full station with the second temperature probe mounted at the top of the tower.

48
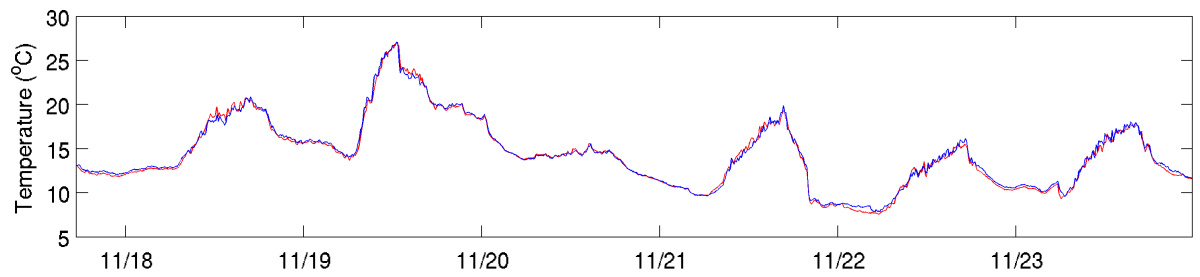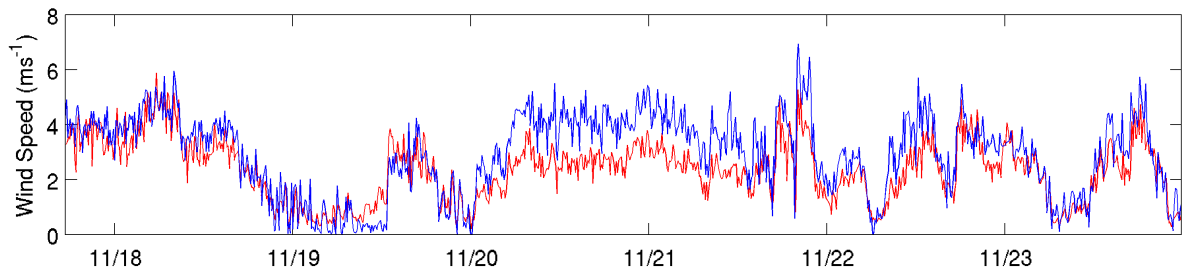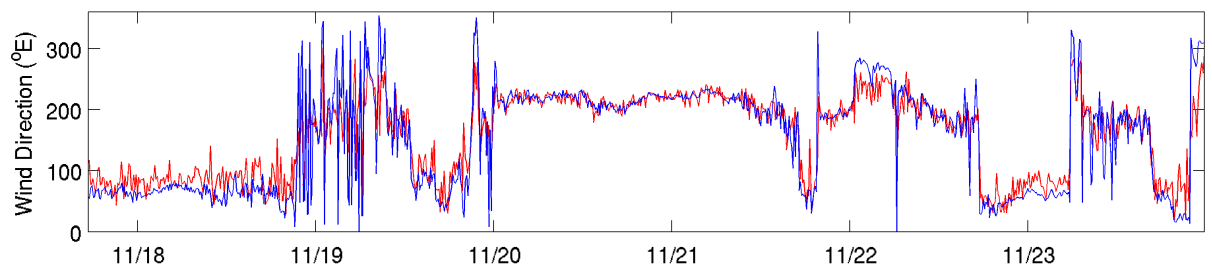
Figure 4.3: Comparison of the reference weather station (red) with the Geography department's weather station (blue) for: (a) temperature; (b) wind speed; (c) wind direction.

4.5.1 Performance of the reference weather station

Figure 4.4 shows the temperature, pressure and wind measurements from the reference weather station during its deployment in Antarctica. All the variables display typical behaviour for calm summer Antarctic conditions. Comparing Figure 4.4a with Figure 4.4c shows that the temperature is higher at altitude during calm conditions, hence suggesting a temperature inversion is formed during these conditions. The combination of large batteries and a solar charger ensured that the weather station had no problems with its power supply.

4.5.2 Initial results from the SNOW-WEB trials

Figure 4.5 shows the locations of the ten SNOW-WEB nodes deployed in Antarctica. These nodes took about a week to deploy completely and the network was left running for a further week. Data from the network spans from the 18th to the 29th of January, although not all the nodes ran continuously for this time because of network testing. A sample of the output can be seen in Figure 4.6a, which shows temperature data for six different stations over a four day span. While slightly different patterns are seen in the temperatures due to geographical separation, the general trend in temperatures is similar over the six nodes. It should also be noted that this diagram shows the sporadic nature of SNOW-WEB node measurements over time. Figure 4.6b shows a composite of the temperature measurements from the ten nodes with the temperature data from the reference weather station. Several SNOW-WEB nodes were deployed before the reference weather station was deployed so there is no reference data for those few days, but the nodes show good agreement with reference values for the days when both were operating. There is some divergence between the reference station and the SNOW-WEB nodes, but this is to be expected due to the geographical distance between nodes. These data also highlight the often sporadic nature of the SNOW-WEB data due to failures in the communication capabilities of the SNOW-WEB nodes. Local data logging largley solved these issues at the end of the deployment.

It must be noted that the temperature is often overestimated by the SNOW-WEB nodes here. In calm and bright conditions, the temperature is often measured as above 0°C, even though this does not agree with reference measurements. This is likely due to inadequate radiation shielding of the temperature sensors, possibly linked to the high albedo of snow reflecting more thermal radiation towards the temperature sensors. Therefore, a redesign of the radiation shields is required for the next Antarctic field season.

Despite the deficiencies in the data acquired from the SNOW-WEB, the field campaign was determined to be successful. Since the network was operational and both successfully logging data and communicating for a large proportion of the time, the SNOW-WEB exceeded the conservative expectations for the field campaign.

4.5.3 Future work using SNOW-WEB data

While the original aim of the field campaign was to acquire enough in situ wind measurements to attempt to determine how winds around Ross Island may affect the sea ice in the Ross Sea, little work was actually carried out on this particular aspect of the research. Due to a
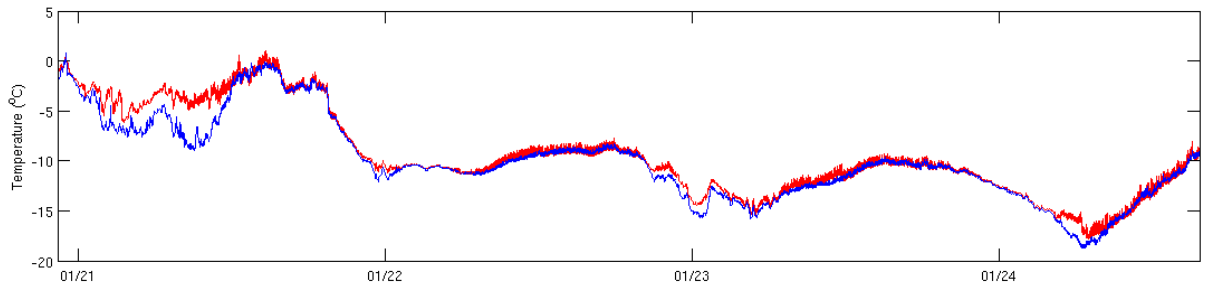
(a)
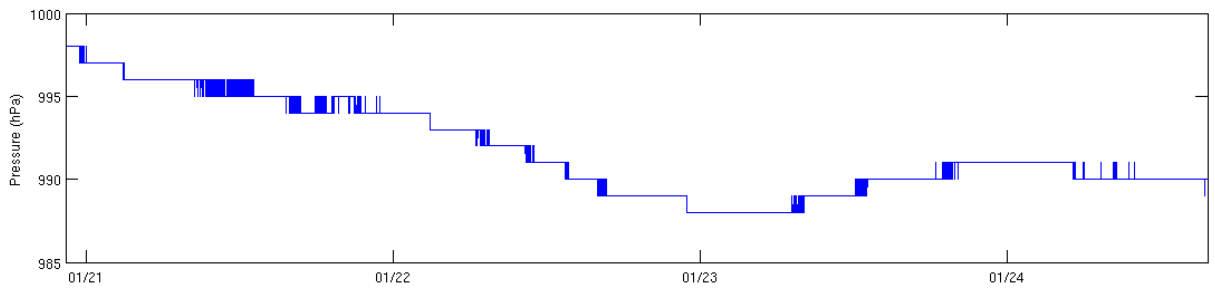
(b)
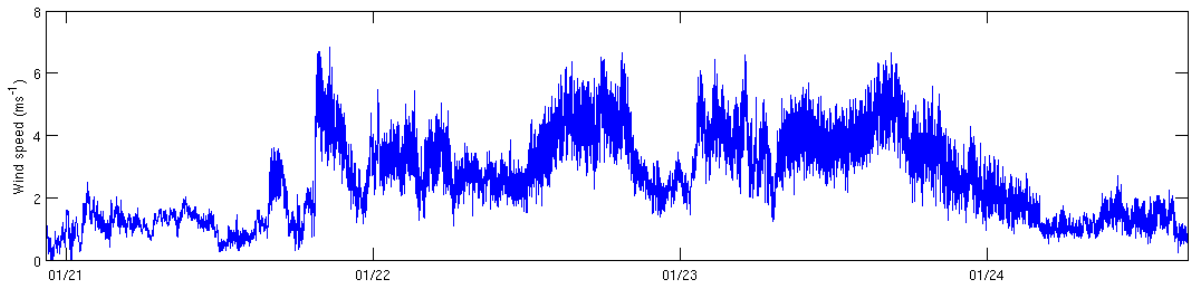
(c)
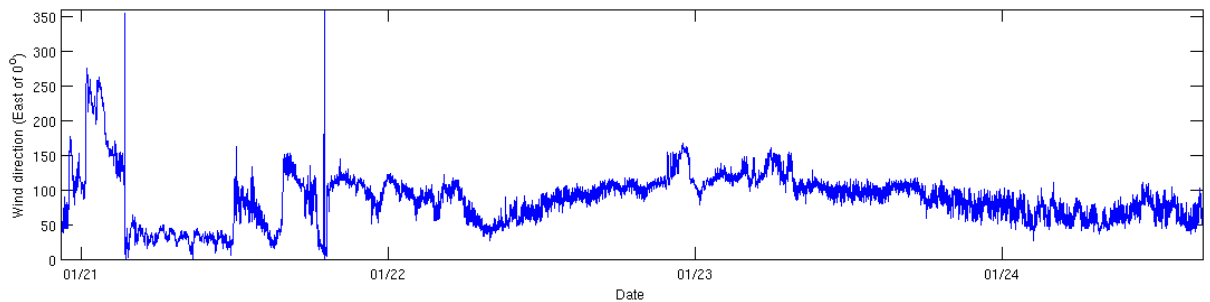
(d)

Figure 4.4: Weather data for four of the eight days deployment of the reference weather station. (a) temperature at 2m (blue) and 6m (red), (b) pressure, (c) wind speed, (d) wind direction.

51
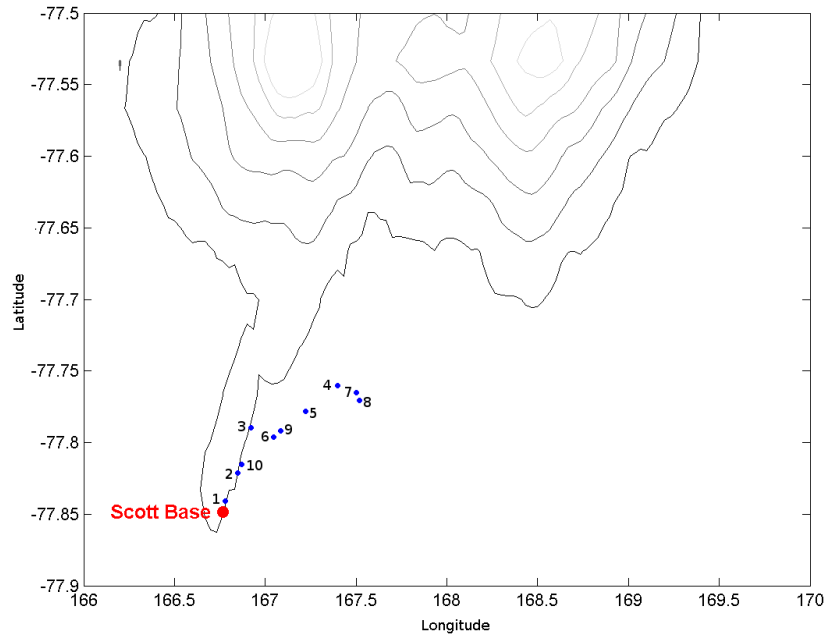
Figure 4.5: Locations of the ten SNOW-WEB nodes deployed near Ross Island in Antarctica, labelled in order of deployment. Base camp and the reference weather station were located at node 4.

combination of a lack of data obtained, more work being done on the other aspects of sea ice analysis and significant disruption to the university year due to the February 22 earthquakes, this area of the sea ice analysis became low-priority and unfeasible .

This work was to have examined the pattern of winds around Ross Island for the time the stations were deployed. By comparing and correlating these winds to the known sea ice behaviour in the Ross Sea for this time, potential conclusions, if any, were to have been found as to how the small scale wind patterns may have influenced the sea ice.
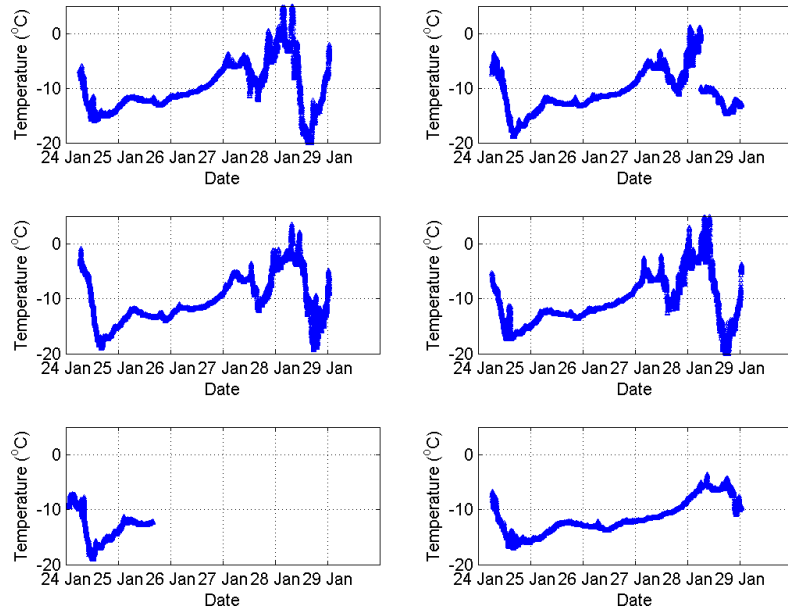
(a)
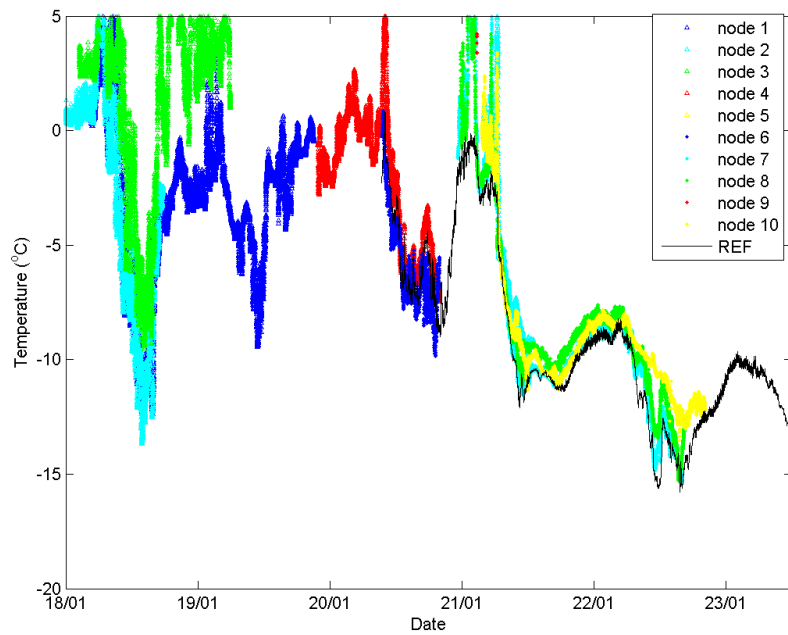
(b)

Figure 4.6: (a) Sample temperature data from six SNOW-WEB nodes from January 25-29 2011. (b) Comparison between SNOW-WEB data (coloured) and the reference weather station (black). SNOW-WEB nodes further away from the station display increasing divergence from the reference data, as is expected. The

53

Chapter 5

Conclusions

The elliptical diagnostic technique described in this study for measuring and analysing Antarctic sea ice is potentially advantageous because it provides a method for studying sea ice behaviour in terms of a simple mathematical model. This model allows both the total sea ice area and the geographic variations in the sea ice cover to be quantified in terms of the ellipse parameters. This method provides an integrated measure of sea ice and does not rely on dividing the sea ice into arbitrary sectors which has previously been done (Zwally et al., 1983). It is potentially useful due to its ability to capture sea ice variations in a simpler and more complete manner than traditional total and regional sea ice extent analysis. The five parameters that define an ellipse describe the ellipse centroid coordinates, the lengths of the major and minor axes and the rotation angle of the major axis of the ellipse. The combination of these parameters allows the geographic distribution of the sea ice to be easily quantified. In particular, the rotation angle of the major axis of the ellipse is a useful measure to allow this quantification. This is advantageous because several previous studies have indicated that the spatial variability of Antarctic sea ice responds to external forcings more significantly on regional scales than hemispheric scales (Gloerson et al., 1993; Zwally et al., 2002).

The seasonal patterns in the ellipse parameters agree well with previous sea ice studies (Cavalieri and Parkinson, 2008a) in describing the annual variations in sea ice cover. In particular, the total sea ice areas calculated from the ellipses consistently match those calculated directly from the satellite data used, and these ellipse areas display very similar seasonal patterns to those calculated from the satellite data (Figure 2.3). In addition, the ellipse parameters calculated from all three datasets used compare very well (Figure 3.1a), with correlation coefficients very close to unity (Figure 2.4). One weakness of the model is its performance during the summer months when sea ice is at a minimum. During this period of the year, the sea ice no longer resembles an ellipse and its shape is instead dominated by the Antarctic coastline. The model therefore produces unreliable results for this period of the year, but since the elliptical diagnostic model nevertheless consistently describes the sea ice extent well for the rest of the year, it can be regarded as a useful tool in future sea ice analysis.

Examining the anomalies in the ellipse parameters reveals structures that are apparent in all three datasets (Figure 3.1b). Since these structures do not appear in the total sea ice area measurements but instead in the individual ellipse parameters, this suggests that while

the total Antarctic sea ice extent is relatively insensitive to external forcings, it experiences geographic shifts in the sea ice cover in response to these forcings. Further analysis reveals that these responses are at least partially associated with the large scale teleconnection patterns, namely the ENSO and SAM.

A composite analysis was performed on the sea ice ellipses to determine the likely factors that cause major geographic shifts in the sea ice cover. This analysis shows that El Niño and La Niña events consistently cause large regional responses that agree with previous studies (Yuan and Martinson, 2000, 2001), namely that the sea ice in the Ross and Amundsen Seas experiences decreases and the sea ice in the Weddell Sea experiences increases during El Niño events, and vice versa for La Niña events. There is no such obvious pattern for geographic shifts due to SAM events. However it must be emphasised that this analysis is somewhat incomplete as it has not been performed for purely the ENSO or purely the SAM. However, the initial composite analysis presented shows that the ENSO is the dominant atmospheric circulation mode that causes changes in the sea ice geographic distribution. The composite analysis highlights the main potential advantage of using elliptical diagnostics in studies of Antarctic sea ice, namely that regional variations in the sea ice extent can be easily quantified without dividing the sea ice into arbitrary regions. The analysis performed shows that while the change in total sea ice extent between years is often small, the geographic shift of the sea ice extent is significantly larger. This aspect of sea ice behaviour is not apparent when using traditional total sea ice extent measurements.

Performing lag correlation analysis on the ellipse parameters displays somewhat different results. The correlations between the ENSO and the sea ice ellipse parameters show that only the eccentricity and rotation angle of the ellipses have any significant correlation with the ENSO, however there are extensive correlations seen between the sea ice and the SAM. The positive correlation between the ENSO and the ellipse eccentricity has the effect of increasing the sea ice cover in the Weddell Sea and decreasing the sea ice cover in the Ross Sea during El Niño events, agreeing with both the composite analysis performed here and previous studies of the regional sea ice response to ENSO (Yuan and Martinson, 2000, 2001). The significant correlations between the sea ice cover and the SAM are not readily seen in the composite analysis, but since the correlation analysis here does not take into account the magnitude of the changes caused by the SAM, the differing results from these two analyses are not necessarily contradictory. What this suggests is that while the changes caused in response to SAM forcings do not typically display large magnitudes, they are very consistent. Conversely, the regional changes seen in response to the ENSO are not consistent, but they can display far larger magnitudes.

While initial results form the elliptical diagnostic analysis are promising and suggest that the combination of integrated and regional variations described by the model are advantageous to future Antarctic sea ice studies, the analysis performed on the ellipse parameters is incomplete due to time constraints and multiple significant disruptions to the research caused by the September 2010, February 2011 and June 2011 Christchurch earthquakes.

As part of this work, an in situ method of measuring the impact of localised atmospheric flows on sea ice was developed. The SNOW-WEB project is a long-term project undertaken to develop a network of remote weather stations that can communicate wirelessly in order to monitor atmospheric conditions at very high spatial and temporal resolutions. One of the

intended uses of the SNOW-WEB is to measure surface winds around the edge of the Ross Sea in order to examine the conclusions drawn in Turner et al. (2009) about increased southerly winds in the Ross Sea driving increased sea ice production and northwards advection. The first generation of SNOW-WEB nodes were deployed between Scott Base and Windless Bight in Antarctica during January 2011 for initial field testing. While significant problems were encountered in the initial deployment of the SNOW-WEB and subsequent network testing, several days of continuous measurements were taken for the wind velocities, temperatures, pressures and relative humidities along the span of the network. In addition, a research grade weather station was assembled and deployed coincident to a SNOW-WEB node to act as a reference measurement in order to calibrate the SNOW-WEB network. This station performed without issues for its entire deployment.

While the original aim of the SNOW-WEB trials was to gather enough local wind measurements to attempt to examine the conclusions in Turner et al. (2009), a combination of insufficient data, disruptions caused by the February 2011 earthquake and more work being done on other aspects of sea ice analysis prevented significant work being performed on the SNOW-WEB measurements.

Since much of the analysis is incomplete, a high priority for future work is to complete this analysis to further examine the initial conclusions drawn about the relative importance of ENSO and SAM on the Antarctic sea ice cover. This analysis can then be combined with measurements from the SNOW-WEB network to examine the relative importance of small-scale atmospheric forcings on the sea ice extent in the Ross Sea. Fraser Dennsion, another postgraduate student in the atmospheric research group is applying the elliptical diagnostic model to examine the quality of sea ice data produced by various general circulation models (GCMs). So far, his research has shown that no GCM adequately reproduces sea ice extents which produce sets of ellipse parameters that match observations. One possible use of the elliptical diagnostic model is therefore providing a method to mathematically model the shape of the sea ice cover throughout the year for GCM sea ice data output.

Appendix A

Mathematics of the Ellipse Fitting Algorithm

The specific algorithm used to fit the ellipse is described in Taubin (1991) and summarised here. The algorithm is non-iterative so is computationally efficient.

The general equation for an ellipse can be written as:

$$Ax^2 + Bxy + Cy^2 + Dx + Ey + F = 0 \tag{A.1}$$

where $A, \ldots, F$ are the unknown coefficients of the ellipse. To fit an ellipse as accurately as possible, $A, \ldots, F$ must be computed to minimise the algebraic distance J between the data given by (x_α, y_α) and the curve:

$$J = \frac{1}{N} \sum_{\alpha=1}^{N} \left(Ax_\alpha^2 + Bx_\alpha y_\alpha + Dx_\alpha + Ey_\alpha + F \right)^2 \tag{A.2}$$

The unknown coefficients are written in a vectorial form and then can be normalised:

$$u = \begin{pmatrix} A & B & C & D & E & F \end{pmatrix}^T \tag{A.3}$$

$$(u, \mathbf{N}u) = \text{constant} \tag{A.4}$$

for some symmetric matrix $\mathbf{N}$. If the weighted matrix $\mathbf{N}$ is given, the solution u that minimises Equation A.1 is immediately computed. Given that:

$$\xi = \begin{pmatrix} x^2 & 2xy & y^2 & x & y & 1 \end{pmatrix}^T \tag{A.5}$$

Equation A.1 can be written as:

$$(u, \xi) = 0 \tag{A.6}$$

If ξ_α is the value of ξ for (x_α, y_α), then Equation A.2 becomes:

$$J = \frac{1}{N} \sum_{\alpha=1}^{N} (u, \xi_\alpha)^2 = \frac{1}{N} \sum_{\alpha=1}^{N} u^T \xi_\alpha \xi_\alpha^T u = (u, Mu) \tag{A.7}$$

where M is defined as:

$$M = \frac{1}{N} \sum_{\alpha=1}^{N} \xi_\alpha \xi_\alpha^T \tag{A.8}$$

Since Equation A.7 is quadratic in u, it is minimised by solving the generalised eigenvalue problem

$$Mu = \mu \mathbf{N} u \tag{A.9}$$

where μ here is the generalised eigenvalue. The solution for the ellipse fitting is given by the generalised eigenvector u for μ with the smallest absolute value. Taubin (1991) gives the weighted matrix $\mathbf{N}$ as:

$$\mathbf{N}_T = \frac{1}{N} \sum_{\alpha=1}^{N} \begin{pmatrix} x_\alpha^2 & x_\alpha y_\alpha & 0 & x_\alpha & 0 & 0 \\ x_\alpha y_\alpha & x_\alpha^2 + y_\alpha^2 & x_\alpha y_\alpha & y_\alpha & x_\alpha & 0 \\ 0 & x_\alpha y_\alpha & y_\alpha^2 & 0 & y_\alpha & 0 \\ x_\alpha & y_\alpha & 0 & 1 & 0 & 0 \\ 0 & x_\alpha & y_\alpha & 0 & 1 & 0 \\ 0 & 0 & 0 & 0 & 0 & 0 \end{pmatrix} \tag{A.10}$$

so the coefficients of the fitted ellipse are given by the unit generalised eigenvector u for the smallest generalised eigenvalue μ. We can then convert the coefficients of Equation A.1 into the parameters required:

Centroid coordinates:

$$x_0 = \frac{CD - BE}{B^2 - AC} \tag{A.11}$$

$$y_0 = \frac{AE - BD}{B^2 - AC} \tag{A.12}$$

Minor axis length:

$$a' = \sqrt{\frac{2(AE^2 + CD^2 + FB^2 + 2BDE - ACF)}{(B^2 - AC)\left[\sqrt{(A-C)^2 + 4B^2} - (A+C)\right]}} \tag{A.13}$$

Major axis length:

$$b' = \sqrt{\frac{2(AE^2 + CD^2 + FB^2 + 2BDE - ACF)}{(B^2 - AC)\left[-\sqrt{(A-C)^2 + 4B^2} - (A+C)\right]}} \tag{A.14}$$

Rotation angle:

$$\theta = \begin{cases} 0 & \text{for } B = 0 \text{ and } A < C \\ \frac{1}{2}\pi & \text{for } B = 0 \text{ and } A > C \\ \frac{1}{2}\cot^{-1}\left(\frac{A-C}{2B}\right) & \text{for } B \neq 0 \text{ and } A < C \\ \frac{\pi}{2} + \frac{1}{2}\cot^{-1}\left(\frac{A-C}{2B}\right) & \text{for } B \neq 0 \text{ and } A > C \end{cases} \tag{A.15}$$

Bibliography

J. R. Allen and D. G. Long. Microwave observations of daily Antarctic sea-ice edge expansion and contraction rates. *IEEE Geoscience and Remote Sensing Letters*, 3:54–58, 2006.

O. Arzel, T. Fichifet, and H. Goosse. Sea ice evolution over the 20th and 21st centuries as simulated by current AOGCMs. *Ocean Modelling*, 12:401–415, 2006.

AVR ATMEGA64 Data Sheet 2490L–AVR–10/06. Atmel Corporation, a. URL `http://www.atmel.com`.

AVR AT45DCB008D Datasheet 3607E–DFLASH–01/08. Atmel Corporation, b. URL `http://www.atmel.com`.

E. Bjorgo, O. M. Johannessen, and M. W. Miles. Analysis of merged SSMR-SSMI time series of Arctic and Antarctic sea ice parameters 1978-1995. *Geophysical Research Letters*, 24: 413–416, 1997.

H. Bonekamp, A. Sterl, and G. J. Komen. Interannual variability in the Southern Ocean from an ocean model forced by European Centre for Medium-Range Weather Forecasts reanalysis fluxes. *Journal of Geophysical Research-Oceans*, 104(C6):13317–13331, 1999.

BP 380 80 Watt Photovoltaic Module Datasheet. BP Solar USA. URL `http://www.bpsolar.com`.

M. I. Budyko. Effect of solar radiation variations on climate of earth. *Tellus*, 21:611–619, 1969.

CR1000 Measurement and Control System Operator's Manual. Campbell Scientific, Incorporated, a. URL `http://www.campbellsci.com`.

SR50 A/AT Sonic Ranging Sensor. Campbell Scientific, Incorporated, b. URL `http://www.campbellsci.com`.

D. J. Cavalieri and C. L. Parkinson. Antarctic sea ice variability and trends, 1979–2006. *Journal of Geophysical Research - Oceans*, 113(19), 2008a.

D. J. Cavalieri and C. L. Parkinson. Arctic sea ice variability and trends, 1979–2006. *Journal of Geophysical Research - Oceans*, 113(19), 2008b.

D. J. Cavalieri, P. Gloerson, C. L. Parkinson, J. C. Comiso, and H. J. Zwally. Observed hemispheric asymmetry in global sea ice changes. *Science*, 278:1104–1106, 1997.

D. J. Cavalieri, C. L. Parkinson, and K. Y. Vinnikov. 30-Year satellite record reveals contrasting Arctic and Antarctic decadal sea ice variablility. *Geophysical Research Letters*, 30 (4), 2003.

W. L. Chapman and J. E. Walsh. Recent Variations of Sea ice and Air Temperature in High Latitudes. *Bulletin of the American Meteorological Society*, 74:33–47, 1993.

M. Christoph, T. P. Barnett, and E. Roeckner. The Antarctic Circumpolar Wave in a coupled ocean-atmosphere GCM. *Journal of Climate*, 11(7):1659–1672, 1998.

J. C. Comiso. Sea ice microwave emissivities from satellite passive microwave and infrared observations. *Journal of Geophysical Research*, 88:7686–7704, 1983.

J. C. Comiso. Bootstrap Sea Ice Concentrations from Nimbus-7 SMMR and DMSP SSM/I. Digital media, 1999, updated 2008. URL `http://nsidc.org/data/nsidc-0079.html`. Boulder, Colorado USA: National Snow and Ice Data Center.

J. C. Comiso. Variability and Trends in Antarctic Surface Temperatures from In Situ and Satellite Infrared Measurements. *Journal Of Climate*, 13:1674–1696, 2000.

J. C. Comiso and F. Nishio. Trends in the sea ice cover using enhanced and compatible AMSR-E, SSM/I and SMMR data. *Journal of Geophysical Research - Oceans*, 113, 2008.

J. A. Curry, J. L. Schramm, and E.E. Ebert. Sea-Ice Albedo Climate Feedback Mechanism. *Journal of Climate*, 8:240–247, 1995.

Deutsches Hydrographisches Institute. *Atlas of ice conditions in the North Atlantic Ocean and general charts of the ice conditions of the Nort and South Polar regions.* Publication 2335, Hamburg, Germany, 1950.

DiaMec Ultra SB1692 12V 40Ah Sealed Lead Acid Battery Datasheet. DiaMec Industrial Battery, Limited, a. URL `http://www.diamec.com.hk`.

DiaMec Ultra SB2487 12V 9Ah Sealed Lead Acid Battery Datasheet. DiaMec Industrial Battery, Limited, b. URL `http://www.diamec.com.hk`.

XBee/XBeePro OEM RF Modules Product Manual v1.xAx - 802.15.4 Protocol. Digi International, Incorporated. URL `http://www.digi.com`.

L. Dubach and C. Ng. *NSSDC's Compendium of Meteorological Space Programs, Satellites and Experiments.* National Space Science Data Center, 1988.

G. M. Flato and G. J. Boer. Warming asymmetry in climate change simulations. *Geophysical Research Letters*, 28(195–198), 2001.

P. Gloerson. Modulation of Hemispheric Sea-Ice Cover by ENSO Events. *Nature*, 373: 503–506, 1995.

P. Gloerson and W. J. Campbell. Recent variations in Arctic and Antarctic sea-ice covers. *Nature*, 352:33–36, 1991.

P. Gloerson, W. J. Campbell, D. J. Cavalieri, J. C. Comiso, C. L. Parkinson, and H. J. Zwally. Satellite passive microwave observations and analysis of Arctic and Antarctic sea-ice. *Annals of Glaciology*, 17, 1993.

J. E. Graf, W. Y. Tsai, and L. Jones. Overview of QuikSCAT mission - a quick deployment of a high resolution, wide swath scanning scatterometer for ocean wind measurement. In *IEEE Southeastcon - Conference Proceedings*, pages 314–317, 1998.

A. Hall and M. Visbeck. Synchronous variability in the southern hemisphere atmosphere, sea ice and ocean resulting from the annular mode. *Journal of Climate*, 15:3043–3057, 2002.

S. A. Harangozo. A search for ENSO teleconnections in the west Antarctic Peninsula climate in austral winter. *International Journal of Climatology*, 20(6):663–679, 2000.

S. A. Harangozo and W. M. Connolley. The role of atmospheric circulation in the record minimum extent of open water in the Ross Sea in the 2003 austral summer. *Atmosphere-Ocean*, 44(1):83–97, 2006.

JW-O-24001-12-9 Wireless Booster Antennae Datasheet. Jinghua Communication Company, Limited. URL `http://www.gzjinghua.com/`.

K. Kanatani and P. Rangarajan. Hyper least squares fitting of circles and ellipses. *Computational Statistics and Data Analysis*, 55(6):2197–2208, 2011.

H. J. Kramer. *Observation of the Earth and its Environment*. New York: Springer-Verlag, 1994.

R. Kwok and J. C. Comiso. Southern Ocean climate and sea ice anomalies associated with the Southern Oscillation. *Journal of Climate*, 15:3043–3057, 2002.

W. Lefebvre and H. Goosse. An analysis of the atmospheric processes driving the larg-scale winter sea ice variability in the Southern Ocean. *Journal of Geophysical Research*, 113, 2008.

W. Lefebvre, H. Goosse, R. Timmermann, and T. Fichifet. Influence of the Southern Annular Mode on the sea ice–ocean system. *Journal of Geophysical Research*, 109, 2004.

J. P. Liu, X. J. Yuan, D. Rind, and D. G. Martinson. Mechanism study of the ENSO and southern high latitude climate teleconnections. *Geophysical Research Letters*, 29(4), 2002.

J. P. Liu, J. A. Curry, and D. G. Martinson. Interpretation of recent Antarctic sea ice variability. *Geophysical Research Letters*, 31, 2004.

D. G. Long. NASA SCP Arctic and Antarctic Ice Extent from QuikSCAT, 1999-2004. Digital media, 2004. URL `http://nsidc.org/data/nsidc-0265.html`. Boulder, Colorado USA: National Snow and Ice Data Center.

D. G. Long, P. J. Hardin, and T. Whiting, P. Resolution Enhancement of Spaceborne Scatterometer Data. *IEEE Transactions on Geosciences and Remote Sensing*, 32(3):700–715, 1993.

E. N. Lorenz. The nature and theory of the general circulation of the atmosphere. *World Meteorological Organisation*, 1967. WMO monograph 218.

C. R. Madrid, editor. *The Nimbus 7 Users' Guide*. Goddard Space Flight Center, NASA, 1978.

G. J. Marshall. Trends in the Southern Annular Mode from observations and reanalyses. *Journal of Climate*, 16:4134–4143, 2003. URL `http://www.antarctica.ac.uk/met/gjma/sam.html`. Accessed on 1.8.11.

D. G. Martinson and R. A. Iannuzzi. Spatial/temporal patterns in Weddell gyre characteristics and their relationship to global climate. *Journal of Geophysical Research*, 108(C4): 8083, 2003.

#200P Wind Vane Datasheet. NexGen Wind, Limited. URL `http://www.nexgenwind.com`.

NRG #40H Anemometer, Hall Effect Datasheet. NRG Systems, Limited. URL `htp://www.nrgsystems.com`.

PCF8583 Clock and Calendar Datasheet. NXP Semiconductors. URL `http://www.nxp.com`.

Y. H. Park. Interannual sea level variability in the Southern Ocean within the context of global climate change. *AVISO Newsletter*, 8:95–96, 2001.

Y. H. Park, F. Roquet, and F. Vivier. Quasi-stationary ENSO wave signals versus the Antarctic Circumpolar Wave scenario. *Geophysical Research Letters*, 31(5), 2004.

C. L. Parkinson and D. J. Cavalieri. A 21 year record of Arctic sea-ice extents and their regional, seasonal and monthly variability and trends. *Annals of Glaciology*, 34:441–446, 2002.

C. L. Parkinson, J. C. Comiso, H. J. Zwally, D. J. Cavalieri, P. Gloerson, and W. J. Campbell. Arctic sea ice 1973–1976 from satellite passive microwave observations. *NASA Special Publications*, (489):296, 1987.

C. L. Parkinson, D. J. Cavalieri, P. Gloerson, H. J. Zwally, and J. C. Comiso. Arctic sea ice extents, areas, and trends, 1978-1996. *Journal of Geophysical Research*, 104(C9):20837–20856, 1999.

B. Qiu and F. F. Jin. Antarctic Circumpolar Waves: An indication of ocean-atmosphere coupling in the extratropics. *Geophysical Research Letters*, 24(21):2585–2588, 1997.

Model 41003 Multi-Plate Radiation Shield Instruction Sheet. R. M. Young Company, a. URL `http://www.rmyoung.com`.

Model 41342VC/VF Platinum Temperature Probe Instruction Sheet. R. M. Young Company, b. URL `http://www.rmyoung.com`.

Model 85004 Ultrasonic Anemometer (heated) Instruction Manual. R. M. Young Company, c. URL `http://www.rmyoung.com`.

M. N. Raphael. The influence of atmospheric zonal wave three on Antarctic sea ice variability. *Journal of Geophysical Research*, 112(D12), 2007.

N. A. Rayner, E. B. Parker, C. K. Horton, L. V. Folland, D. P. Alexander, E. C. Rowell, E. C. Kent, and A. Kaplan. Global analyses of sea surface temperature, sea ice, and night marine air temperature since the late nineteenth century. *Journal of Geophysical Research*, 108(D14), 2003.

T. E. Reddy, K. R. Arrigo, and D. M. Holland. The role of thermal and mechanical processes in the formation of the Ross Sea sumemr polynya. *Journal of Geophysical Research*, 112, 2007.

Q. P. Remund. Sea Ice Extent Mapping Using Ku-band Scatterometer Data. *Journal of Geophysical Research*, 104(C5):11515–11527, 1999.

Q. P. Remund and D. G. Long. Sea Ice Mapping Algorithm for QuikSCAT and SeaWinds. *Proceedings of the International Geoscience and Remote Sensing Symposium*, pages 1841–1843, 1998. Seattle, WA, 4-8 August 1997.

Q. P. Remund and D. G. Long. Iterative Estimation of Antarctic Sea Ice Extent Using Sea-Winds Data. *Proceedings of the International Geoscience and Remote Sensing Symposium*, pages 491–493, 2000. Honolulu, HI, 24-28 July 2000.

D. Rind, M. Chandler, J. Lerner, D. G. Martinson, and X. Yuan. The climate response to basin-specific changes in latitudinal temperature gradients and the implications for sea icer variability. *Journal of Geophysical Research*, 106(D17):20161–20173, 2000.

S. R. Rintoul, S Sokolov, and R. A. Massom. Rapid development and persistence of a massive Antarctic sea ice tongue. *Journal of Geophysical Research*, 113, 2008.

A. Sen Gupta and M. H. England. Coupled ocean-atmosphere-ice response to variations in the Southern Annular Mode. *Journal of Climate*, 19:4457–4486, 2006.

SHT7x Humidity and Temperature Sensor Datasheet. Sensirion, Incorporated. URL `http://www.sensirion.com`.

I. Simmonds and T. H. Jacka. Relationships between the interannual variability of Antarctic sea ice and the Southern Oscillation. *Journal of Climate*, 8:637–647, 1995.

Soanar EcoTech ZM9091ECO Monocrystalline 12V 5W Solar Panel Datasheet. Soanar EcoTech, Limited. URL `http://www.soanarecotech.com`.

S. Solomon, D. Qin, M. Manning, Z. Chen, M. Marquis, K. B. Averyt, M. Tignor, and H. L. Miller. *Climate Change 2007, The Physical Science basis. Contribution of Working Group 1 to the Fourth Assessment Report of the Intergovernmental Panel on Climate Change*, chapter 3: Observations: Surface and Atmosphere Climate Change, pages 235–336. Cambridge University Press, 2007.

S. E. Stammerjohn, D. G. Martinson, R. C. Smith, X. Yuan, and D. Rind. Trends in Antarctic annual sea ice retreat and advance and their relation to El Niño-Southern Oscillation and Southern Annular Mode variability. *Journal of Geophysical Research-Oceans*, 113(20), 2008.

J. Stroeve, M. M. Holland, W. Meier, T. Scambos, and M. Serreze. Arctic sea ice decline: Faster than Forecast. *Geophysical Research Letters*, 34(5), 2007.

G. Taubin. Estimation of planar curves, surfaces and nonplanar space curves defined by implicit equations with applications to edge and range image segmentation. *IEEE Transactions on Pattern Analysis and Machine Intelligence*, 13:1115–1138, 1991.

D. W. J. Thompson and S. Solomon. Interpretation of Recent Southern Hemisphere Climate Change. *Science*, 296(5569):895–899, 2002.

E. I. Tolstikov, editor. *Atlas of the Antarctic*, volume 1. Ministerstvo Geologii SSSR, 1966.

Copernicus II GPS Receiver Datasheet. Trimble Navigation Limited. URL http://www.trimble.com.

J. Turner and J. Overland. Contrasting climate change in the two polar regions. *Polar Research*, 28:146–164, 2009.

J. Turner, J. C. Comiso, G. J. Marshall, T. A. Lachlan-Cope, T. Bracegirdle, T. Maksym, M. P. Meredith, Z. Wang, and A. Orr. Non-annular atmospheric circulation change induced by stratospheric ozone depletion and its role in the recent increase of Antarctic se aice extent. *Geophysical Research Letters*, 36, 2009.

Y. Udagawa, Y. Tachibana, and K. Yamazaki. Modulation in interannual sea ice patterns in the Southern Ocean in association with large-scale atmospheric mode shift. *Journal of Geophysical Research-Atmospheres*, 114, 2009.

PTB210 Digital Barometer User Guide. Vaisala, Incorporated, a. URL http://www.vaisala.com.

SPH20 Static Pressure Head User Guide. Vaisala, Incorporated, b. URL http://www.vaisala.com.

VTI SCP1000 Series Absolute Pressure Sensor Datasheet. VTI Technologies Oy. URL http://www.vti.fi.

J. E. Walsh. The role of sea ice in climate variability: theories and evidence. *Atmosphere-Ocean*, 21:229–242, 1983.

J. E. Walsh. A comparison of Arctic and Antarctic climate change, present and future. *Antarctic Science*, 21:179–188, 2009.

D. W. Waugh. Elliptical diagnostics of stratospheric polar vortices. *Quarterly Journal of the Royal Meteorological Society*, 123:1725–1748, 1997.

W. B. White and R. G. Peterson. An Antarctic circumpolar wave in surface pressure, wind, temperature and sea-ice extent. *Nature*, 380:699–702, 1996.

W. B. White, S. C. Chen, and R. G. Peterson. The Antarctic circumpolar wave: A beta effect in ocean-atmosphere coupling over the Southern Ocean. *Journal of Physical Oceanography*, 28(12):2345–2361, 1998.

T. Wilheit. *Nimbus-5 Users' Guide*. NASA/Goddard Space Flight Center, 1972.

K. Wolter. The Southern Oscillation in surface circulation and climate over the tropical Atlantic, eastern Pacific, and Indian Oceans as captured by cluster analysis. *Journal of Climate and Applied Meteorology*, 26:540–558, 1987. URL `http://www.esrl.noaa.gov/psd/enso/mei/`. Accessed on 1.8.11.

K. Wolter and M. S. Timlin. Monitoring ENSO in COADS with a seasonally adjusted principal component index. *Proceedings of the 17th Climate Diagnostics Workshop*, pages 52–57, 1993.

X. J. Yuan and C. H. Li. Climate modes in high southern latitudes and their impacts on Antarctic sea ice. *Journal of Geophysical Research-Oceans*, 113(13), 2008.

X. J. Yuan and D. G. Martinson. Antarctic sea ice extent variability and its global connectivity. *Journal of Climate*, 13:1697–1717, 2000.

X. J. Yuan and D. G. Martinson. The Antarctic Dipole and its predictability. *Geophysical Research Letters*, 28:3609–3612, 2001.

H. J. Zwally, C. L. Parkinson, and J. C. Comiso. Variability of Antarctic Sea Ice and Changes in Carbon Dioxide. *Science*, 220:1005–1012, 1983.

H. J. Zwally, J. C. Comiso, C. L. Parkinson, D. J. Cavalieri, and P. Gloerson. Variability of Antarctic Sea Ice 1979–1998. *Journal of Geophysical Research - Oceans*, 107(C5), 2002.